Thermodynamic Modeling of Mg-Al-Ca System

FARHANA ISLAM

A Thesis in
The Department of Mechanical and Industrial Engineering

Presented in Partial Fulfillment of Requirements
For the Degree of Master of Applied Science (Mechanical Engineering) at
Concordia University
Montreal, Quebec, Canada.

September 15, 2004

Your file Votre référence
ISBN: 0-612-94726-2
Our file Notre référence
ISBN: 0-612-94726-2

Abstract

Thermodynamic modeling of Mg-Al-Ca system

Farhana Islam

Research on magnesium alloys is fuelled by the need for low-density, high specific strength materials that suit aerospace and automobile industries. Consequently applications of Mg alloys are expanding to critical components where higher creep and corrosion resistance at elevated temperature (>150°C) are required. Hence, development of phase relations of Mg alloy systems is essential for further development.

This study develops a Mg-Al-Ca ternary system from three binary systems: Mg-Ca, Al-Ca and Mg-Al. Of these three binaries, the optimized data for Al-Mg system are taken from the most recent and reliable COST 507 database. In this study, the other two systems, Mg-Ca and Al-Ca, are thermodynamically modeled and optimized with fewer model parameters by considering the experimental phase equilibria and thermodynamic data available in the literature. The calculated results from this study agree well with the experimental values. From the set of optimized model parameters of the three binary systems, a self-consistent thermodynamic database including all phases is constructed.

A complete Mg-Al-Ca ternary system is constructed from this database. The isothermal sections, liquidus projections, phase assemblage diagrams, vertical sections for specific compositions and all possible invariant points are calculated for this ternary system. This database offers a useful tool for the development of new alloys and better understanding of their behavior.

Acknowledgements

First of all, I would like to express my special gratitude and thanks to my thesis supervisor Dr. Mamoun Medraj for his invaluable guidance, assistance and cooperation leading up to the finishing of this research work. Dr. Medraj's suggestions have been of enormous help to throughout the period of my research.

I am also thankful to my research teammates for their helps and comments. Thanks to the faculty members and administrators of mechanical engineering department for providing a congenial environment that has facilitated completing my academic and research work.

Finally I wish to thank my husband Nobbir Ahmed and my parents and my sisters and brothers for all their inspiration and encouragement.

Table of contents

List of figures

List of tables

CHAPTER I

Introduction

Magnesium was discovered in 1774 and named after the ancient city Magnesia. It is found to be the 8th most abundant element in the earth's crust and third most plentiful element dissolved in seawater. It is not found in elemental form in nature but only in the chemical combinations. It is the lightest metal for structural application having a density of only 1.74 g/cm^3 weighing only two-thirds as much as aluminum (2.70 g/cm^3) and over four times lighter than iron (7.86 g/cm^3) and steel. Its melting temperature is 650°C and has a close-packed hexagonal (HCP) crystal structure [1, 2].

In spite of these promising properties, the application of Mg is still behind that of competing materials such as aluminum and plastics. The reasons behind this are:

- fairly high priced base material,
- low ductility and yield strength,
- poor cold working ability due to low strain hardening,
- high degree of shrinkage, which leads to microporosity,
- restriction to further processing like welding due to porosity,
- low rigidity and corrosion resistance and high reactivity.

For these reasons, attempts have been made to improve the characteristics of magnesium alloys by employing different alloying elements. In this way, all the advantageous properties listed below have been realized.

- Lowest density of all construction metals; light construction parts possible,
- high specific strength (strength/density ratio),
- excellent castability, steel dies may be used,
- good machinability (milling, turning, sawing),
- improved corrosion resistance with high purity alloys,
- high damping properties,
- integrated recycling possible.

These desirable attributes enable magnesium to economically replace many zinc and aluminum die-casting as well as cast iron and steel components and assemblies in automotive industries. The potential for the application of shaped magnesium parts in vehicle is great; as shown in Figure 1.1, the majority of the body shape consists entirely of formed parts, representing almost 25% of the vehicle weight.

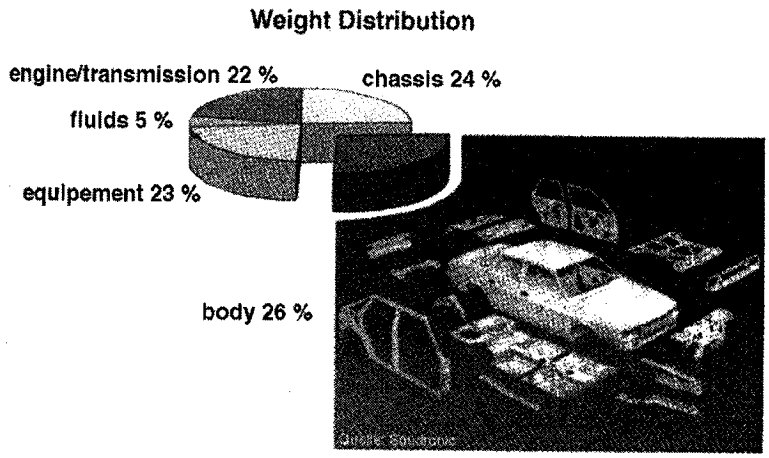

Figure 1.1: *Use of magnesium sheet in automotive engineering [3]*

During both world wars the expansion of the aircraft industry and the demand for flares, billets, and incendiary devices brought a rapid development in magnesium technology. In the last decade magnesium has made significant application in automotive industry at room or near room temperature. The world consumption of magnesium alloys in the automobile industry has experienced an 18% annual increase from 1990 to 1996 a 32% increase from 1996-1997 and an annual growth rate of 8% is anticipated until 2020 [11]. Nowadays, the automotive industry leads the way in the growing interest in Mg alloys in order to decrease fuel consumption and to reduce emissions. It is evident that the largest saving in weight could be achieved by constructing the most massive components, such as engine blocks, cylinder head, gear box casing etc. But the poor creep resistance and high cost of commercial magnesium alloys have prevented magnesium application in major power train components such as engine blocks and automatic transmission cases, where operating temperature can be as high as 250°C and 175°C, respectively. The construction material of these components has to be thermally and dimensionally stable during the lifetime of the vehicle. Thus this material has to be resistant to creep. For such applications, recent efforts have been made to develop inexpensive creep resistant magnesium alloys based on Mg-Al system [1, 2, 4, 5].

1.1 Magnesium and its alloys

Since the advent of magnesium alloys, there has been a lot of effort to influence the properties of pure magnesium with different alloying elements. The main mechanism for improving the mechanical properties is precipitation hardening and/or solid solution hardening.

By the 1920s aluminum had already become the most important alloying element for magnesium to enhance both mechanical (tensile strength and hardness) and corrosion properties. The hardness effect was caused by precipitating γ-phase ($Mg_{17}Al_{12}$) and was only observed up to 120°C. Besides the improvement of the mechanical properties, there is the big advantage of better castability (eutectic temperature, T_E = 437°C). Due to these reasons most technical alloys, especially casting alloys, contain a high percentage of aluminum. However the use of Mg-Al alloys is limited to low temperature applications. Therefore a large effort has been made to increase the service temperature of these alloys [6, 3, 7].

Addition of rare earth metals to Mg-Al alloys can improve creep resistance. But they all are too expensive to use in the mass automotive industry. On the other hand their creep resistance is not sufficiently good for use in modern liquid cooled engines. Some attempts were made to replace rare earth metals by Ca but die sticking and hot cracking are still problems to be solved. Recently developed Mg-Al-Ca based alloys containing small additions of strontium and/or silicon offer excellent creep resistance (under both tensile and compressive stresses) at elevated temperature and low cost which meet the materials requirements for automotive power train applications [4]. The Al content can be high compared to Si-containing alloys, which leads to better castability. The improved creep resistance is attributed to the thermal stability and the interfacial coherency of the $(Mg,Al)_2Ca$ phase in the microstructure of the alloys [8]. Pekguleryuz and Renaud [9] mentioned that diecast Mg-Al-Ca alloys offer creep resistance, tensile strength and corrosion resistance comparable to commercially used Mg-alloys with rare earth additions. Moreover, calcium protects melt surface causing less slag formation and less

additive loss. Figure 1.2 shows the influence of Ca addition to AE42, AS21 and Mg-Al-Ca alloys to improve mechanical properties. Table 1.1 shows the chemical composition of different alloys used in Figure 1.2.

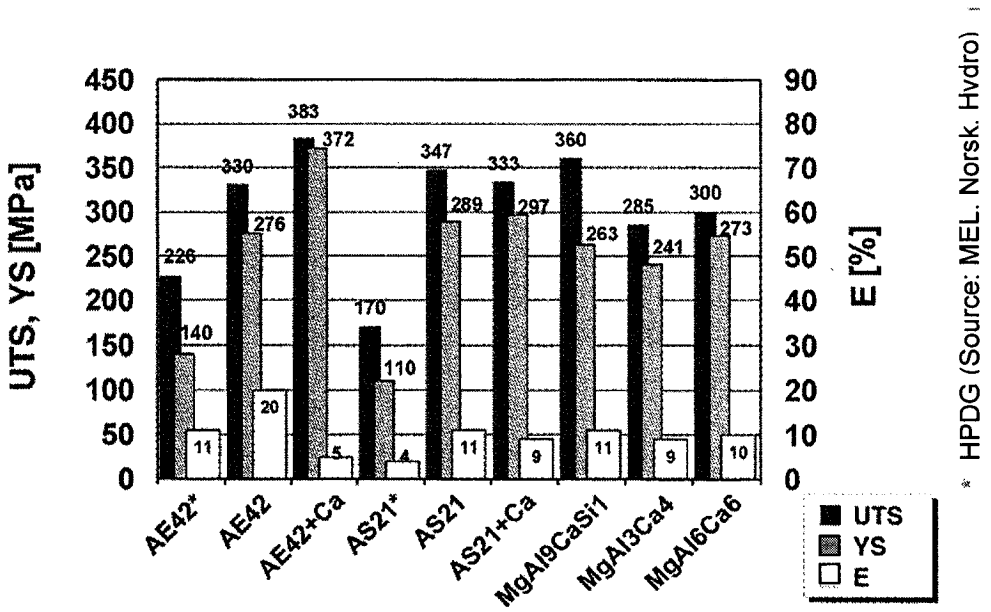

Figure 1.2: *Mechanical properties of different Mg alloys (tensile strength, yield strength, elongation at fracture) at room temperature [3]*

Table 1.1: *Composition of different alloys in wt% [3]*

Alloys	Al	Ca	Mn	SE*	Si
AE42	4.2			1.5	
AE42+Ca	4.0	5.6		1.3	
AS21		2.9	0.25		1
AS21+Ca	3.2	4.4			0.9
MgAl9CaSi1	9.5	4.3			1.1
MgAl3Ca4	3.4	4.3			
MgAl6Ca6	9.4	6.2			

SE*=Nd-rich rare earth elements or mixed metal

1.2 Creep behavior of Mg alloy

The characteristics of creep behavior of Mg and its alloys are observed due to the following reasons [9,10]:

- The main creep mechanism in Mg alloys, in the stress-temperature ranges of interest for automotive application, is grain boundary sliding. The creep mechanisms of pure Mg at low temperatures are basal slip within the grains and sub-grain formation (transient creep) while at high temperatures diffusion dependent mechanisms of grain boundary deformation and sliding (steady state creep) become predominant. The same type of change was observed to occur as the stress level at a particular high temperature decreases.
- By stress-recovery mechanism, Mg seems to creep even at low temperature. This is mostly sub-grain formation, resulting possibly in a higher density of sub-structures near grain boundaries.
- Aging and precipitation from the supersaturated matrix during creep in some Mg-Al alloys are suspected to be detrimental especially for grain boundary resistance to creep. While in some Mg-Ce alloys dynamic precipitation from the matrix has been suspected to increase creep resistance.

1.2.1 Creep behavior of Mg-Al-Ca alloy

Like pure Mg the Mg-Al alloys also suffer poor creep resistance. The microstructure of these alloys is characterized by the Mg-$Mg_{17}Al_{12}$ eutectic at the grain boundary. The $Mg_{17}Al_{12}$ intermetallic compound is incoherent with the α-magnesium matrix and exists at a wide composition range of 48-52 wt% Al and has a low melting

point (437°C). The compound is therefore, prone to aging, has poor metallurgical stability as the temperature is increased and may contribute to the poor creep resistance [9]. The use of this alloy hence cannot be expanded to transmission and engine components due to insufficient creep resistance at the higher operating temperature. But by adding some other elements, for example Si to Mg-Al alloys, the creep resistance of this alloy can be improved. This is because of the presence of thermally stable Mg_2Si compound in microsturcture.

Figure 1.3 shows the comparison of creep deformation between different AX alloys and, AZ91 and AE42 alloys. It can be noticed that AX has equal or better creep resistance than AE42. The chemical composition of these alloys is shown in Table 1.2.

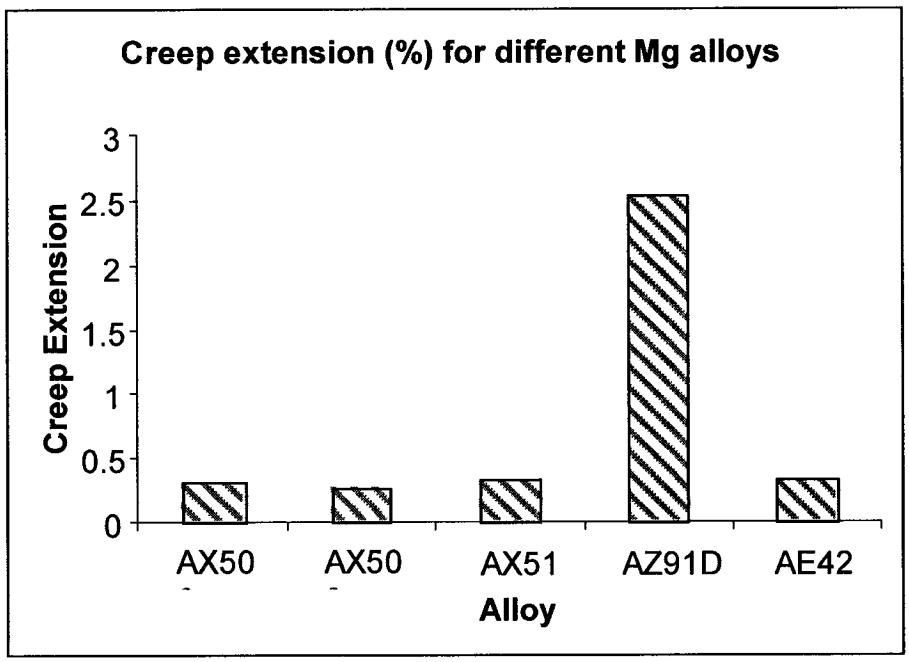

Figure 1.3: *Creep resistance at 150°C, 35Mpa for 200 hrs [9]*

Table 1.2: Chemical composition of the die cast alloys [9]

Alloys	Al (wt %)	Ca (wt %)	Mn (wt %)	Zn (wt %)	Fe (ppm)	Cu (ppm)	Ni (ppm)	Rare earth (wt%)
AX506	4.5	0.6	0.24	0.003	10	2	2	-
AX508	4.5	0.8	0.25	0.003	10	2	<2	-
AX51	4.6	1	0.24	0.003	13	2	<2	-
AZ91D	8.9	-	0.20	0.81	25	7	6	-
AE42	4.1	-	0.29	0.01	38	20	10	2.2

The increased creep resistance of these alloys (AX506, AX508 and AX51) is due to the existence of an Al_2Ca intermetallic compound along the grain boundary in the as-cast structure. It is also stable at high temperature and has a high melting point at 1079°C. It is likely that the thermally stable phase impedes grain boundary sliding and diffusion related dislocation climb at high temperatures and can partly explain the improved creep resistance. Another reason for the improved creep resistance is the absence of low melting point eutectic γ-phase ($Mg_{17}Al_{12}$) and any aging and creep-induced precipitation in the alloy structure at the grain boundary due to the presence of calcium [4, 9].

1.3 Need for developing phase diagram:

The importance of the phase diagram is immense in all aspects of material development. Equilibrium phase diagrams represent the relationships between the temperature, the composition and the quantities of phases at equilibrium. This is why they are frequently used as roadmaps for alloy design or for better understanding of the processing of materials. Phase diagrams are helpful in predicting phase transformations and the resulting microstructures, which may have equilibrium or nonequilibrium character. Ternary phase diagram is a useful tool in understanding the solidification

process of alloys. It also helps to focus on the promising regions – thus avoiding the formation of compound that causes poor creep strength at elevated temperature.

Despite the high potential of Mg-Al-Ca alloy system, the phase diagram is scarcely known. Phase diagrams can be calculated using CALPHAD approach. In this approach the Gibbs energy of individual phases is modeled, and the model parameters are collected in a thermodynamic database. Thermodynamic modeling begins with the evaluation of thermodynamic descriptions of binary systems. By combining thermodynamic descriptions of constitutive binary systems, ternary system can be developed. These descriptions cover the whole composition and temperature ranges including the experimentally uninvestigated regions [11]. In this study the ternary phase diagram of the Mg-Al-Ca system has been calculated from a self-consistent database. This in turn enables better understanding of Mg alloys as well as the development of new alloys in this system.

CHAPTER II

Literature Review

This literature is based on the current research performed on the most promising Mg-Al-Ca system and its three constituent binaries Mg-Ca, Al-Ca and Mg-Al. The experimental and calculated data of the phase diagram and thermodynamic properties of these three binaries have been described in the following sections.

2.1 Mg-Ca system

2.1.1 Equilibrium phase diagram

First Baar [12] determined the complete liquidus temperatures for the Mg-Ca system. In his work the purity of the starting elements was low and there was significant loss of Ca during alloying. Paris [13] also determined the complete liquidus temperature. He obtained a slightly different result from Barr [12] but he did not mention the purity of the materials. Haughton [14] determined the liquidus temperature on Mg-rich alloys in the composition range of 0 to 17% Ca rigorously avoiding loss of Ca. On the other hand Vosskühler [15] analyzed Mg-rich alloys up to 47.65% Ca. The last measurement of the liquidus temperature by Klemm and Dinkelacker [16] agrees fairly well with both of [14] and [15]. Haughton [14] reported that the eutectic reaction occurs on the Mg-rich region at 89.5±0.5 at.% Mg at 790K, compared to Baar's value 87 at.% Mg at 787K and Vosskühler [15], Klemm and Dinkelacker's [16] value 89.5 at.% Mg at 789.5K.

Nayeb-Hashemi and Clark [17] critically evaluated this system. They assessed the phase diagram mainly considering Vosskühler [15], Klemm and Dinkelacker [16] and Baar [12] works. Agarwal *et al.* [18] measured calorimetrically the enthalpies of mixing of liquid Ca-Mg alloy at 1023K and heat contents of Mg_2Ca between 750 and 1150K. They re-optimized the system with these experimental and literature data to verify the compatibility of the results available from different sources. Their calculated Mg-rich eutectic point (89.5 at.% Mg at 790K) and melting temperature of the starting Mg (923K) and Ca (1115K) agrees fairly well with Haughton [14] and Chase [19], respectively. The calculated phase diagram by Agarwal *et al.* [18] is given in Figure 2.1. This diagram shows that the stable phases in Mg-Ca system are: the liquid, the (Mg) solid solution, the Ca-bcc, the Ca-fcc, and the congruent intermetallic compound Mg_2Ca which divides the phase diagram into two eutectic systems. Mg_2Ca is reported in literature as a line compound [17, 18].

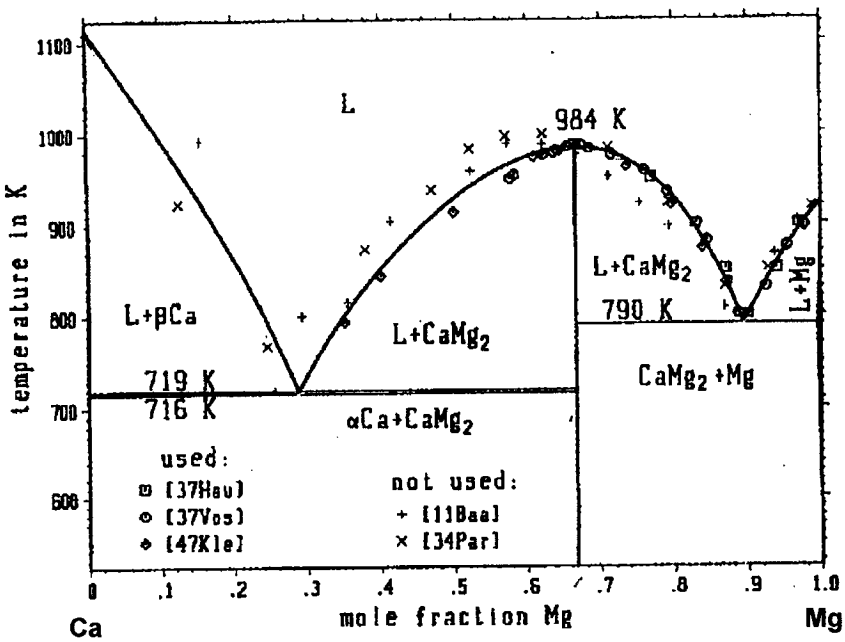

***Figure 2.1**: Calculated Mg-Ca phase diagram [18]*

Several researchers measured the solubility of Ca in Mg [20, 15, 14]. Among them Burke [20] and Vosskühler [15] reported limited solubility and their results agree fairly well, whereas other reported larger solubility. Hence the limited solubility will be considered in this work.

2.1.2 Thermodynamic properties

The standard enthalpy of formation of the compound Mg_2Ca measured by King and Kleepaa [21] using tin solution calorimetry is –40.50±1.25 kJ/mol at 298K. Davison and Smith [22] also measured the enthalpy of formation at room temperature as -39.38 ± 2.63 kJ/mol by acid solution calorimetry and mentioned that the heat of formation determined by King and Kleepaa is "the most precise and probably the most reliable." Later Hultgren *et al.* [23] calculated the value of enthalpy and entropy of formation of Mg_2Ca compound as -13.40 kJ/g-atom and -0.84 J/g-atom.K, respectively.

Sommer *et al.* [24] measured the heat of mixing of liquid Mg-Ca by high temperature calorimtery. Their results are presented in Figure 2.2.

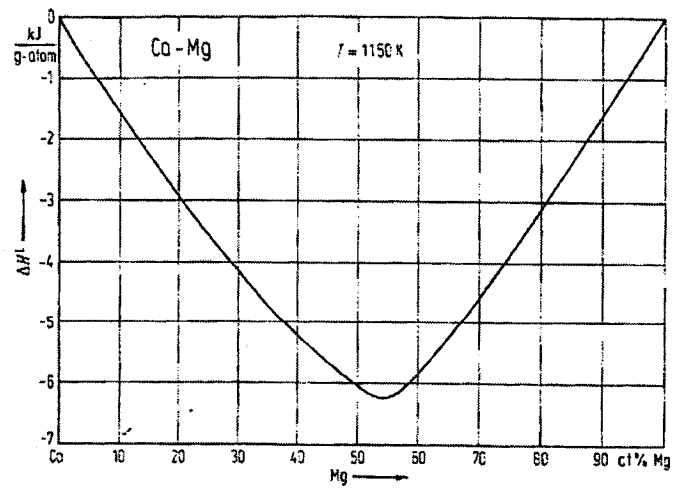

Figure 2.2: *Enthalpy of mixing of liquid Mg and Ca at 1150K [24]*

Although Agarwal *et al.* [18] also measured the enthalpy of mixing calorimetrically at 1023K, their results were not considered in this study because they contradicted those of Sommer *et al.* [24]. However, Mishra *et al.* [25] mentioned that considering energy parameters values at 1023K instead of 1150K could minimize this discrepancy.

Sommer [26], Mashovets and Puchkov [27] and Hultgren *et al.* [23] determined the activity of Mg and Ca by vapor pressure measurement at 1010K and 1200K, respectively. However the activity of Mg reported by [27] is significantly below those of [26]. This can be seen from Figure 2.3. Moreover [27] mentioned that the activity of Ca has a positive deviation from Raoult's law in the Ca-rich region whereas [26] showed a negative deviation. The thermodynamic activities calculated from the primary results of the measurements given by Sommer [26] seem to be more reliable than those published by Mashovets and Puchkov [27] since they [26] are more recent, hence they will be used for the optimization of Mg-Ca system.

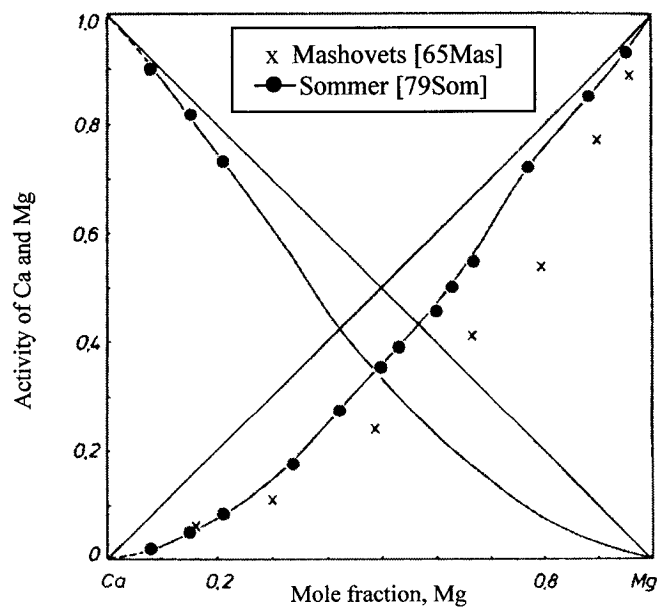

Figure 2.3: *Activity of Ca and Mg in Ca-Mg liquid [26]*

2.2 Al-Ca system

2.2.1 Equilibrium phase diagram

Matsuyama *et al.* [28] investigated the Al-Ca system thoroughly by thermal and thermoresistometric analysis and by microscopic examination. They determined the liquidus line, two eutectic points – one in Al-rich side with the composition of 5.24 at.% Ca at 889K and other is in Ca-rich side with the composition of 65 at.% Ca at 818K. They reported two intermetallic compounds; Al_2Ca, which melts congruently at 1352K, and Al_4Ca, which melts incongruently at 973K.

In the Al-Ca system most experimental investigations mainly deal with Al-rich corner, which is technically interesting for aluminum alloys. Consequently, only limited experimental work for Ca-rich part was reported. Recently, Kevorkov and Schmid-Fetzer [29] investigated the Al-Ca system experimentally and determined the complete phase diagram. They reported two new intermetallic compounds; AlCa, Al_3Ca_8 in addition to the established Al_4Ca and Al_2Ca compounds. Later, Kevorkov *et al.* [30] optimized this system and determined the thermodynamic properties. The Ca-rich part of the phase diagram differs substantially from previous data because of the two newly discovered intermetallic compounds AlCa and Al_3Ca_8 (Figure 2.4). But they did not report the crystal structure of AlCa. The reason behind this was, the slow kinetics of formation of this phase during the peritectic reaction from the very stable Al_2Ca phase prevented the preparation of single-phase sample for the crystallographic investigation. Nevertheless Huang and Corbett [31] reported the occurrence of $Al_{14}Ca_{13}$ compound with monoclinic structure instead of AlCa. Therefore, from the most recent publications [30, 31, 32],

it can be concluded that the stable phases in this system are: the liquid, Al-fcc, Ca-bcc, Ca-fcc and four intermetallic compounds; Al_4Ca, Al_2Ca, $Al_{14}Ca_{13}$, Al_3Ca_8. Among them

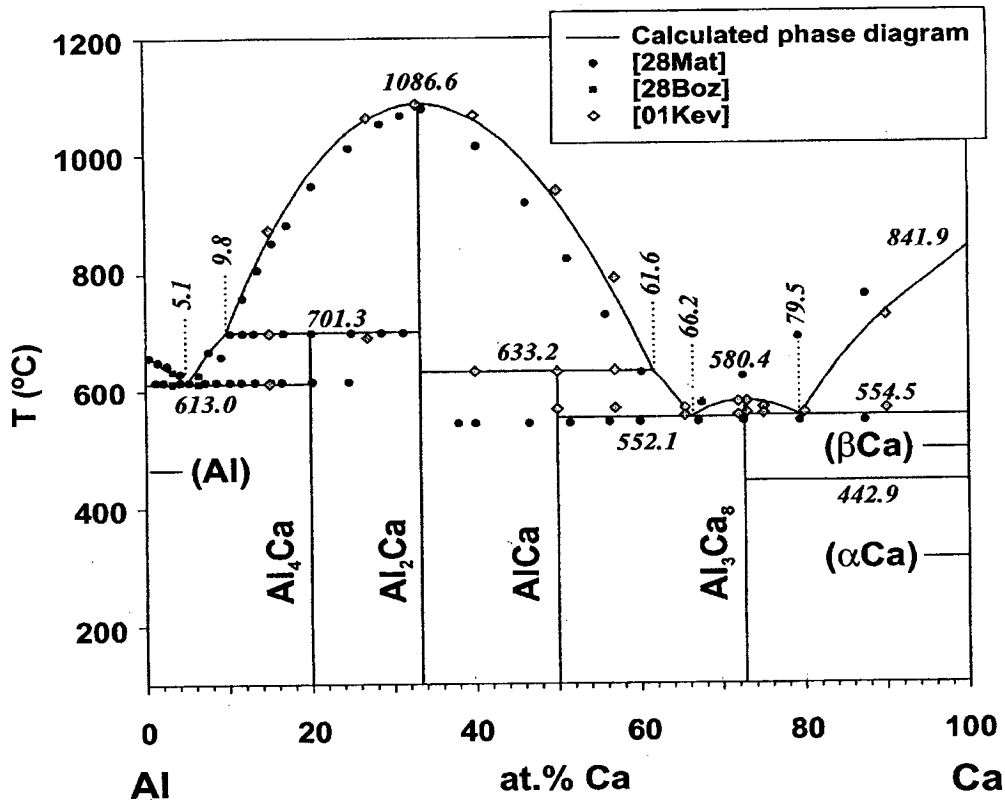

Figure 2.4: *Calculated phase diagram of the Al-Ca system [30]*

Al_4Ca, $Al_{14}Ca_{13}$ melt incongruently forming liquid and Al_2Ca at the peritectic transformation temperatures of 973K and 906K, respectively [32]. Al_2Ca, Al_3Ca_8 melt congruently at 1352K and 850K, respectively. There are two eutectic points on the Ca-rich side instead of one reported by Matsuyama *et al.* [28]. These eutectic reactions occur at around 829K and 833K with compositions of 66.2 and 79.5 at.% Ca, respectively [32]. Nowotny *et al.* [33] determined the crystal structure of Al_4Ca and Al_2Ca as b.c.t and f.c.c, respectively. Whereas Huang and Corbett [31] investigated the crystal structures of $Al_{14}Ca_{13}$ and Al_3Ca_8 using X-ray analysis and mentioned that they have monoclinic and triclinic structure, respectively.

Ozturk *et al.* [32] used both associate and random solution models to re-optimize the system with $Al_{14}Ca_{13}$ intermetallic compound instead of AlCa (Figure 2.5).

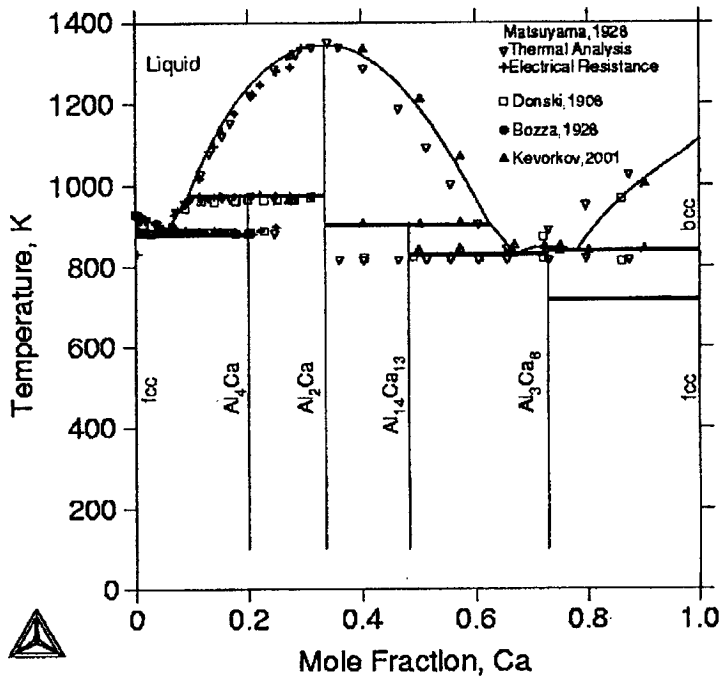

Figure 2.5: *Calculated Al-Ca phase diagram using random solution model, compared with experimental data [32]*

The results from the two models were the same. When the random solution model is used for the liquid phase with Redlich-Kister polynomial, the higher order interaction parameters in the liquid are needed to reproduce the liquidus around the high melting temperature intermetallic compounds like Al_2Ca and it often results in a less satisfactory liquidus at other compositions. In this system there is a tendency for short range ordering and a strong evidences for the existence of molecular like Al_2Ca species that are called associates [32]. But the associate model is not chemically true because in real case the big or large molecule Al_2Ca substitute one atomic position, which is not feasible.

Itkin *et al.* [34] mentioned in his study that the solubility of Ca at 873K was found to be less than 0.03 at.% that agreed with other studies and accepted as a reasonable estimation. Recently, Kevorkov and Schmid-Fetzer [29] mentioned that, during XRD investigation of the Al and Ca-rich alloys no deviation from the theoretical powder patterns were detected. Therefore the solubility regions of Ca in Al and Al in Ca are supposed to be negligible.

2.2.2 Thermodynamic properties

Kevorkov *et al.* [30] determined the partial enthalpy of mixing at infinite dissolution of pure Ca in aluminum by drop solution calorimetry. They reported Δh_{Ca}= -89.9±1.6 kJ/mol at 978K which is in good agreement with the data of Notin *et al.* [35]. Notin *et al.* measured Ca partial enthalpies of mixing by dissolving small amounts of solid Ca in a bath of liquid Al at 953K and 1038K. They also calculated the enthalpies of mixing of liquid solution by integration of these results. Sommer *et al.* [36] used high temperature calorimetry for determining the enthalpy of mixing of liquid at temperatures ranging between 1125K and 1190K. Their experimental results are in good agreement with integral values obtained by Notin *et al.* [35] as well. Ozturk *et al.* [32] compared the calculated enthalpy of mixing data in the liquid phase at 1453K with [35] and [36] as shown in Figure 2.6.

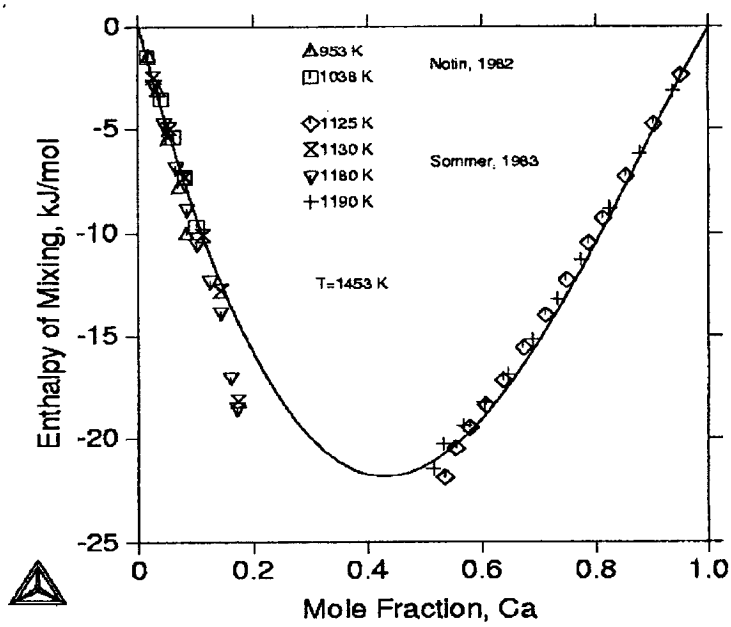

Figure 2.6: *Enthalpy of mixing of Ca and Al in the liquid at 1453K [32]*

Figure 2.6 shows a trend that the minimum of the curve is shifted towards Al side where the most stable intermetallic compound, Al_2Ca, is formed. This indicates strong interactions between the atoms in the liquid at composition around that of the Al_2Ca compound.

Kevorkov *et al.* [30] mentioned that they considered activities and integral enthalpy of mixing data from literature to optimize the thermodynamic parameters of the liquid phase. In order to adjust the liquid phase equilibria to experimental values, their calculated enthalpy of mixing had to deviate from the values reported in the literature as shown in Figure 2.7.

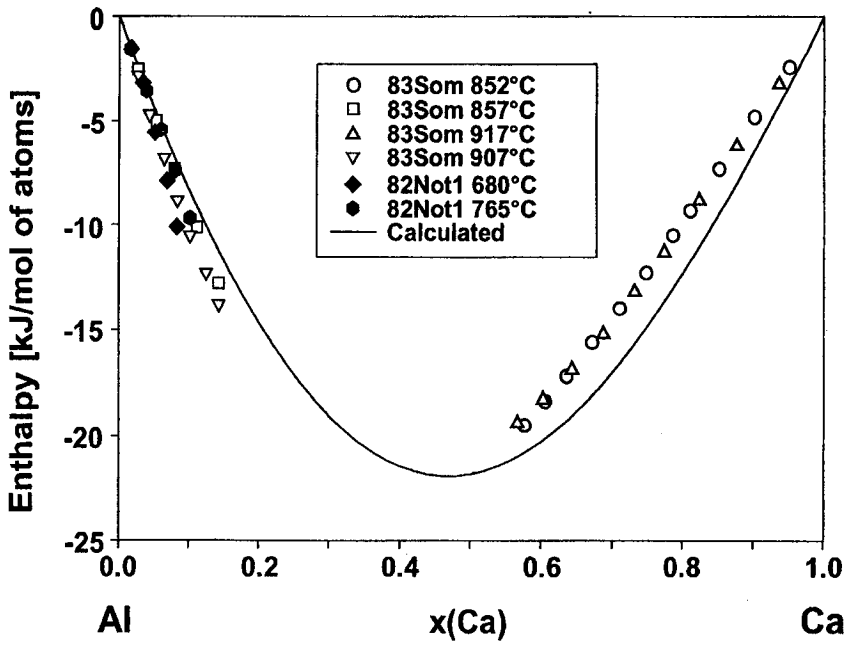

***Figure 2.7**: Enthalpy of mixing of the Al-Ca liquid phase [30]*

They reported that this difference could be minimized. But an attempt to get closer fit may result in shifting of the liquidus line of Al_2Ca to higher temperature on Ca-rich side. Also the eutectic and peritectic temperature will be affected [30].

Jacob *et al.* [37] determined activities in the liquid Al-Ca alloys using Knudsen effusion method for composition range less than 38% and greater than 44% Ca at 1373K. Later they got the activities of the entire composition by combining the results of the two ranges. Schürmann *et al.* [38] calculated the activities of Ca in the liquid alloys by using boiling point determination technique. Kevorkov *et al.* [30] calculated the activity coefficient of Ca, which agrees fairly well with [38] and shows reasonable agreement with [37]. Ozturk *et al.* [32] calculated the activity of Ca at 1600K and compared it with both [37] and [38]. These results can be seen in Figure 2.8.

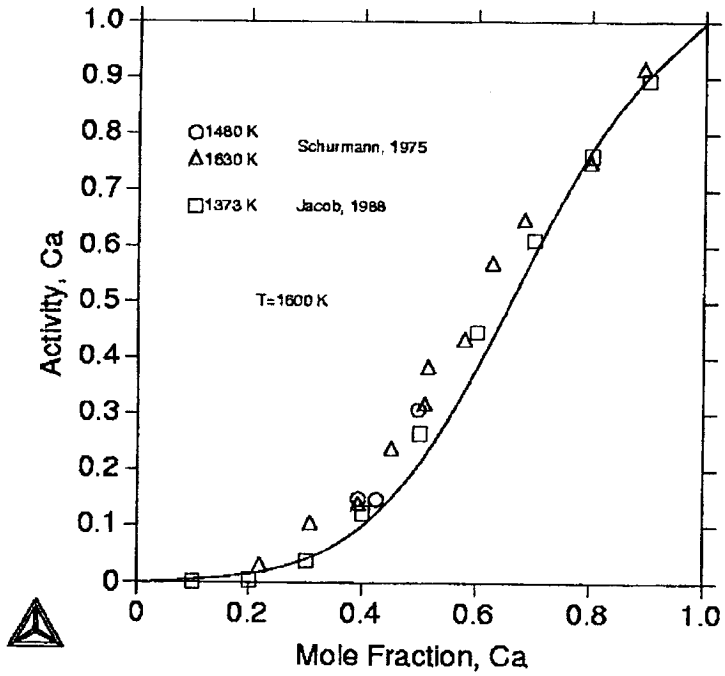

Figure 2.8: *Activities of Ca in the liquid [32]*

Several researchers measured the enthalpy of formation of Al_2Ca and Al_4Ca compounds. Notin *et al.* [35] determined the enthalpy of formation of these compounds at 953K and 1038K more precisely. Each recorded calorimetric signal corresponds to the enthalpy change during the addition of a solid Ca piece to Al melt. There is a reasonable agreement with the values of enthalpy of formation for Al_2Ca between [30] and [35]. The small difference between them may be due to the difference in heat capacity ΔC_p for the formation reaction between room temperature and 1038K [30]. For $Al_{14}Ca_{13}$ intermetallic compound there is no experimental enthalpy of formation data reported in the literature up to date due to the sluggish formation kinetics of the phase and thus difficulty of preparing an $Al_{14}Ca_{13}$-rich sample [32]. The enthalpy of formation of Al_3Ca_8 stoichiometric phase was determined by Kevorkov *et al.* [30] by drop solution calorimetry. For $Al_{14}Ca_{13}$ and Al_3Ca_8 compounds other experimental or calculated values

are not available, as they have been discovered just recently. Gibbs energies and entropies of formation of Al_2Ca and Al_4Ca were also determined using other techniques. For example Notin *et al.* [39] used solid electrolyte galvanic cell technique. The result of the current study will be compared with these different works in Chapter 5.

2.3 Mg-Al system

2.3.1 Equilibrium phase diagram

The Al-Mg system is of particular importance to the aluminum industry and has been the subject of extensive study. There have been several proposals for the Al-Mg phase diagrams; some of them are conflicting mainly in the middle range of concentration. Murray [40] reviewed the work on this prior to 1982 and published the optimized phase diagram shown in Figure 2.9. He stated that the equilibrium phases are: the (Al) solid solution with a maximum Mg solubility of 18.9 at.% at the eutectic temperature; the (Mg) solid solution with a maximum Al solubility of 11.8 at.% at the eutectic temperature; the β solid solution with hexagonal crystal structure; the γ solid solution with the αMn structure; and the R phase with rhombohedral structure at 42 at.% Mg. This R phase is often referred to as ε phase. The atomic radii ratio of Al to Mg is 1.12 that suggests high mutual solid solubility. Murray [40] mentioned that a large amount of Al is available for precipitation and when the Al content exceeds the solubility limit in Mg it forms γ phase. The composition range of β phase has no significant effect on the boundaries because of the narrowness of this phase. He also discussed the crystal structure and lattice parameters of β phase and reported the uncertainty in number of atoms per unit cell.

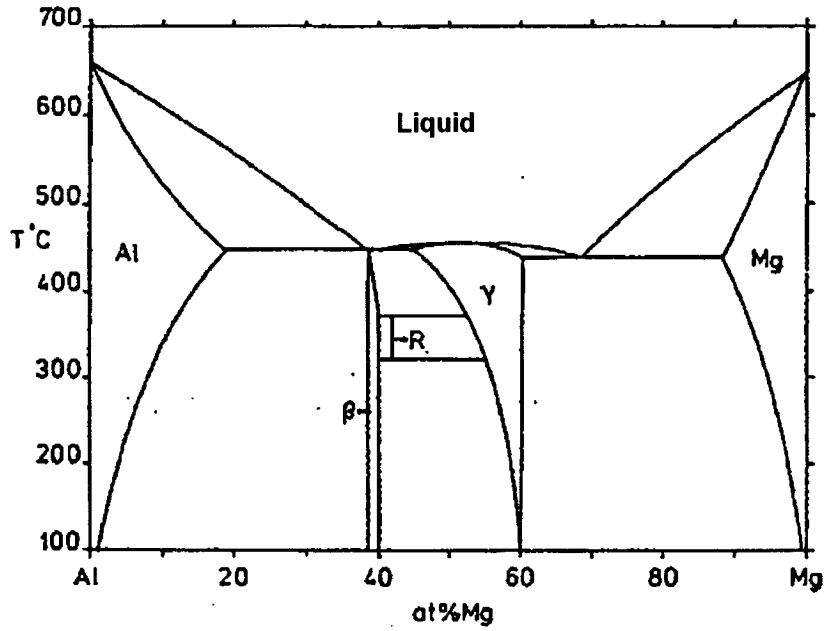

Figure 2.9: *Optimized phase diagram [40]*

Löüdecke and Hack [41] reviewed the chronological development of this system from 1953 to 1982. There is a good agreement between different authors regarding the solid solubility of Mg and Al and liquidus, solidus and solvus lines. But they found that till then there were contradictory results concerning the intermetallic compounds in the concentration range of 40 to 55 at.% Mg.

Saunders [42] reviewed the experimental work of Mg-Al system and carried out a thermodynamic assessment for the Mg-Al system. His calculated phase diagram is shown in Figure 2.10. In addition to β and ε compounds, Saunders considered the presence of ζ phase.

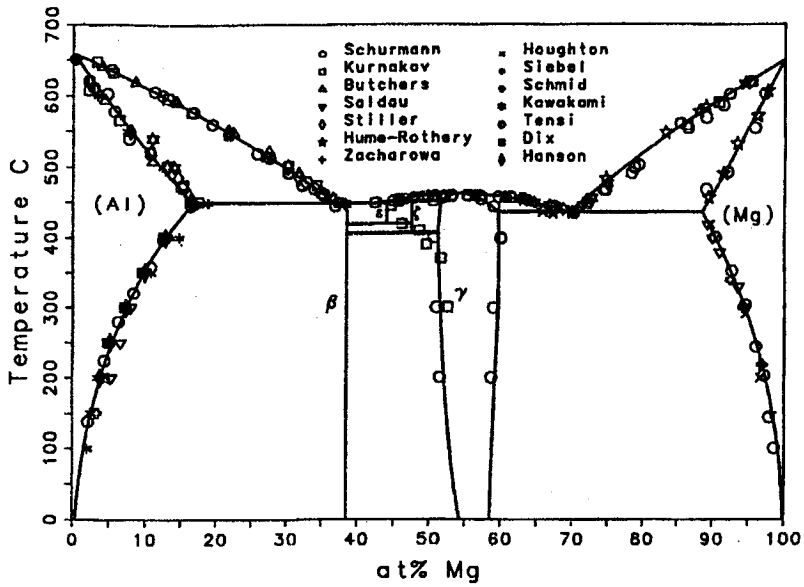

Figure 2.10: *Calculated Al-Mg phase diagram [42]*

Saunders used a sublattice model to assess the central intermetallic γ phase. The solubility range of γ phase at low temperature was found greater than that of Murray [40]. This is because Saunders used a thermodynamic model based on four sublattices, which corresponds to the α-Mn structure of γ phase where Murray used the Wagner-Schottkey model, which is not physically realistic for the γ phase.

Zuo and Chang [43] evaluated the Mg-Al binary system by thermodynamic modeling. The liquid, (Al) and (Mg) were described as disordered solutions and the γ phase was described as an ordered solution phase. The total number of parameters used in this study was 15 compared with 23 used by Saunders and 24 by Murray. In general, a model with fewer parameters is preferred.

In order to obtain more complete and precise results of thermodynamic data on Mg-Al binary system, Chartrand and Pelton [44] decided to re-optimize this system. They used a modified quasi-chemical model for the liquid. Further, they considered a hypothetical β compound as a line compound with formula $Mg_{28}Al_{45}$. Because of the

high discrepancy in activity data of Mg they did not use it during their optimization. But they used it later to check the validity of the calculated values. Their calculated phase diagram (Figure 2.11) agrees fairly well with [40]. There is differences between their optimized values and Saunders [42] and Zuo and Chang [43] due to the inclusion of ζ phase and the use of optimized enthalpy of mixing in these works.

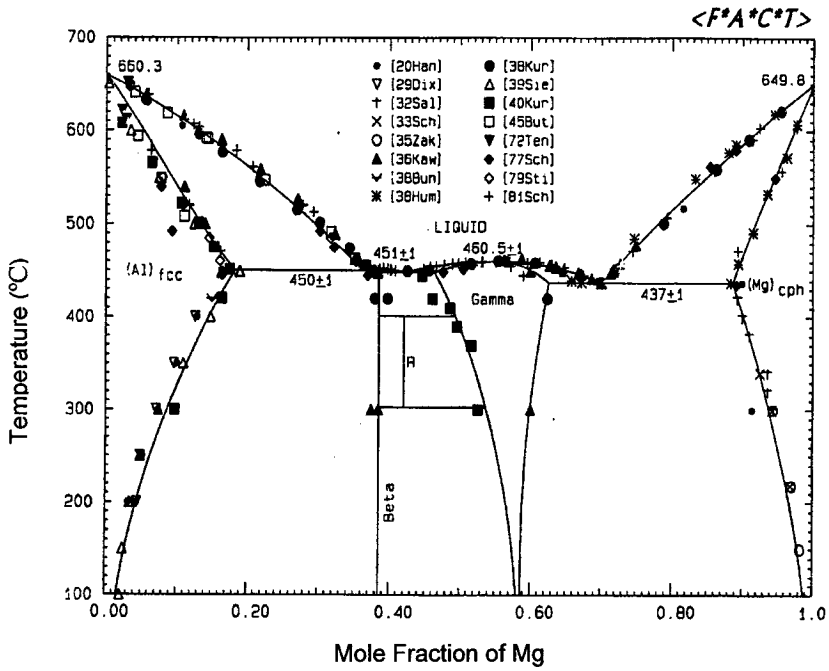

Figure 2.11: *Optimized Mg-Al phase diagram [44]*

Goel *et al.* [45] determined the Mg-Al phase diagram experimentally. Their phase diagram shows good agreement with Murray [40] except for the temperature range of R phase. They proposed that R phase is stable between 305±5°C to 406±5°C instead of 320°C to 370±5°C proposed by Murray [40]. Moser *et al.* [46] determined thermodynamic data for the liquid Al-Mg alloy from emf, vapor pressure and calorimetric studies. The mutual consistency of the data sets for Mg activities was also analyzed in this study. Partial enthalpies of both Mg and Al were also reported.

Su *et al.* [47] performed an experimental investigation of the Mg-Al phase diagram form 47 to 63 at.% Al. They proposed that a high-temperature phase, named λ, exists with a composition between 57 to 58 at.% Al. The rhombohedral ε phase near 56 at.% Al is found to form following a peritectoid reaction (γ+β→ε) at 410°C and not a peritectic reaction as reported in earlier works.

Liang *et al.* [48] experimentally investigated the central part of Mg-Al phase diagram (Figure 2.12). They defined some discrepancies between the experimental data in the composition range of the central part. These discrepancies can be summarized as

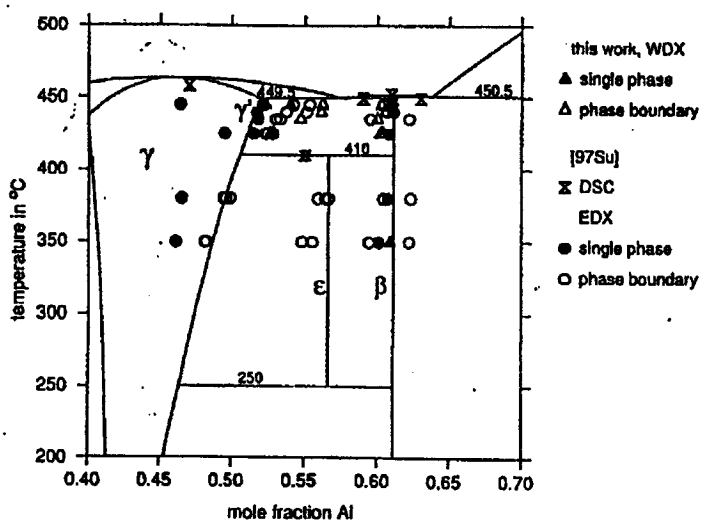

Figure 2.12: *Central part of Mg-Al phase diagram [48]*

the existence of ζ phase, the temperature range of the ε phase and the occurrence of a possible γ′ phase of unknown structure within the γ region. However, they could not give any boundary between γ and γ′ phase and identified that λ phase is a commensurate modulation of the γ phase. They also mentioned that Donnadieu *et al.* [49] showed no existence of this hypothetical λ phase by electron diffraction technique. Moreover, their diagram is not consistent with the diagram reproduced by [44]. Liang *et al.* [48]

suggested that the previous discrepancies on the nature and composition of the intermetallics might be due to the large effect of the cooling rate from the liquid state and the rapid formation of metastable phases in composition range from 47 to 61 at.% Al. They also mentioned that ζ phase ($Al_{49}Mg_{32}$) may be either the sequence of metastable quasi-periodic phases which may occur in this composition range or incommensurately modulated states related to γ phase. In recent investigation most of the researchers adopted the thermodynamic optimization by Liang *et al.* [48].

In most recent work, Czeppe *et al.* [50] mentioned that there was no doubt about the existence of two intermetallic phases: β-Al_3Mg_2 and γ-$Al_{12}Mg_{17}$ (Figure 2.13). But the existence of other phases; stable or metastable in nature suggested by experimental observations were still doubtful. So Czeppe *et al.* [50] verified the temperature and concentration ranges of the stability of the ε phase, as well as thermal stability and possible appearance of other phases in the central part of the equilibrium Mg-Al phase diagram. They studied a part of the Mg-Al phase diagram in the range of composition between 48 and 61 at.% Al by Differential Scanning Calorimetry (DSC).

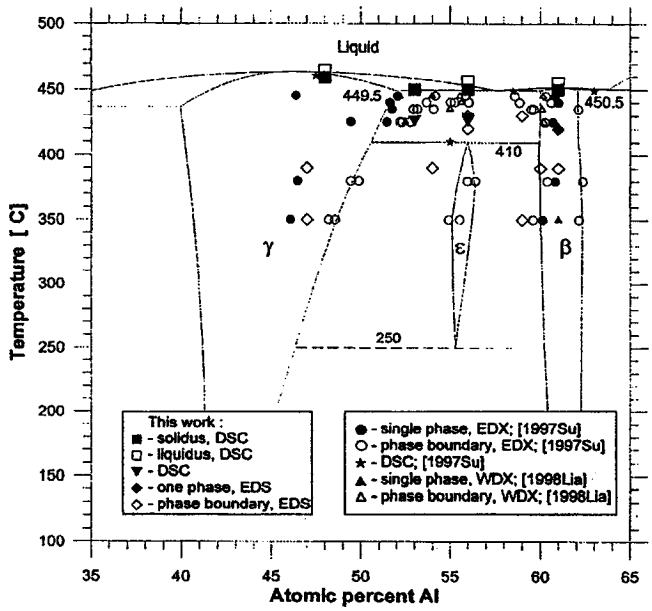

Figure 2.13: *Mg-Al phase diagram [50]; solid/dashed lines are a compilation of data proposed in [47] and [48]*

Czeppe *et al.* [50] mentioned that R or ε phase is located between the β and γ phases with rather wide but uncertain temperature range of stability. The upper temperature limit of the stability of the ε phase was established to be 700±1K. They found that the lower temperature limit of the ε phase formation was not possible, because of the slow reaction $\varepsilon = \beta + \gamma$; further they pointed out that no hypothetical λ, ζ phases were observed, but they showed experimentally that oxide contamination might produce additional thermal effects at temperatures above the stability limit of the ε phase and might falsely suggest the existence of phases other than ε phase in this part of Mg-Al phase diagram.

Ozturk *et al.* [51] mentioned that the precipitation of β phase is the main strengthening mechanism for the Mg-Al based alloys. However β phase has a low melting point and can readily soften and coarsen with increase in temperature due to accelerated diffusion [52].

2.3.2 Thermodynamic properties

The thermodynamic and phase equilibria data of Mg-Al system are important for the production of light, multi-component Mg alloys. The activity of Mg plays an important role in producing cast alloys from secondary materials. Extensive thermodynamic data are available in the literature for liquid Al-Mg alloys, but results from various techniques are not in agreement. An example for the calculated activity of Mg by Chartrand and Pelton [44] is shown in Figure 2.14. All results are scattered and not in good agreement with each other. The reason behind this, according to Moser *et al.* [46], is thermodynamic properties of liquid Mg-Al alloys exhibit only small negative deviations from ideality and are difficult to measure with high accuracy as small heat effects are obtained in calorimetric studies and in emf method. So it is difficult to establish equilibrium at constant temperature [46].

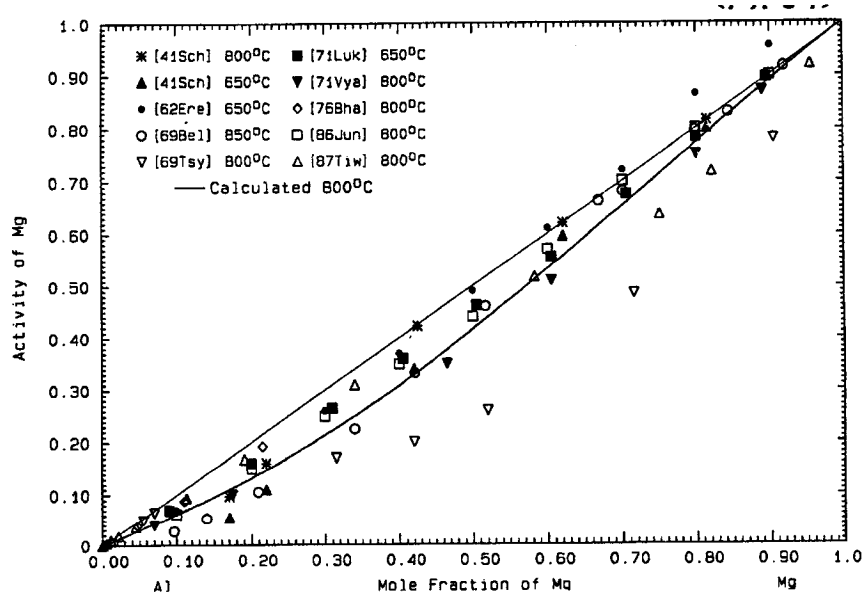

Figure 2.14: *Calculated activity of Mg in Al-Mg liquid alloys at 800°C [44]*

Saunders [42] calculated the enthalpy of mixing for liquid Al-Mg, which was in broad agreement with previous calorimetric measurements (Figure 2.15).

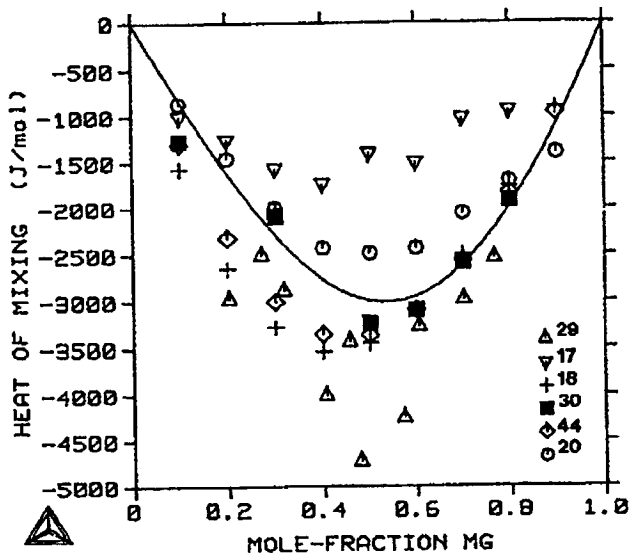

Figure 2.15: *Calculated heat of mixing Mg-Al in liquid phase in relation with experimental results from the literature [42]*

The calculated enthalpy of mixing for liquid Al-Mg by Chartrand and Pelton [44] is presented in Figure 2.16. It is observed from their calculation that the enthalpy values

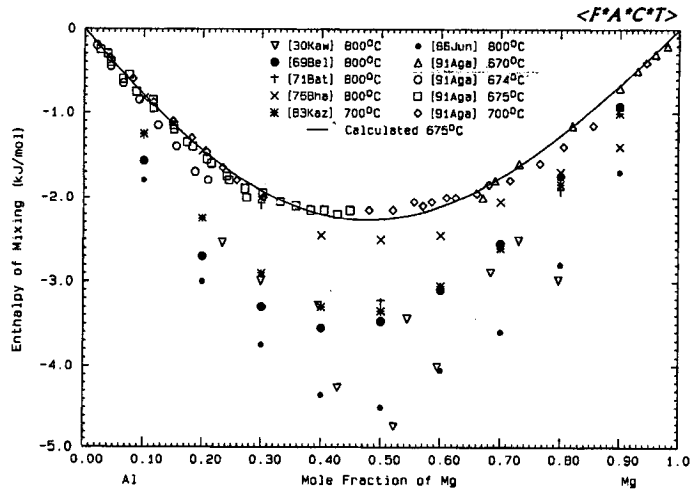

Figure 2.16: *Calculated enthalpy of mixing of Al-Mg alloys at 657°C compared with experimental results from the literatue [44]*

for liquid Al-Mg alloys are higher than the values proposed by Saunders [42]. This is due to the fact that Chartrand and Pelton [44] selected different experimental data in their calculation. Some of the researchers determined the enthalpy of mixing calorimetrically while others derived it from partial pressure and emf method. Systematic errors were minimized in the work of [44] through using the experimental results from three different calorimetric methods.

Moser *et al.* [46] carried out a multi technique research on Mg-Al alloys to determine the consistent thermodynamic data among participating laboratories for the liquid phase and to use those results with the selected information from various references for an optimization and, ultimately, for phase diagram calculations. They reported new thermodynamic data for liquid Mg-Al alloys from emf, vapor pressures and

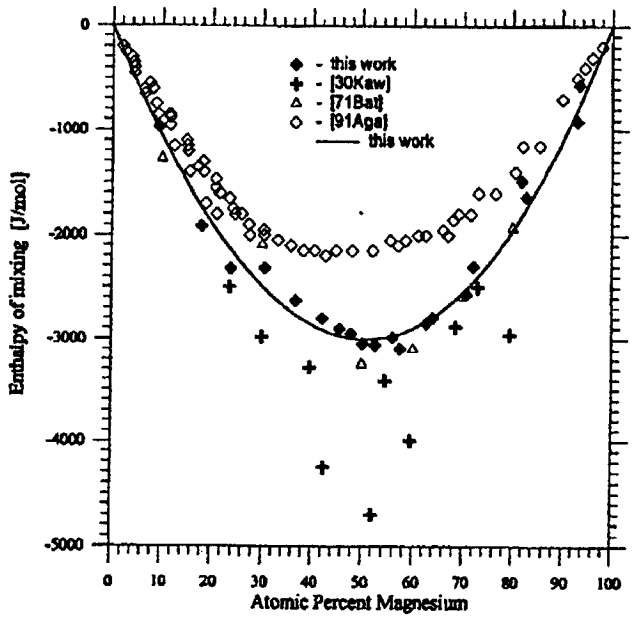

Figure2.17: *Integral enthalpies in liquid Al-Mg alloys [46]*

calorimetric studies and then optimized their results together with the thermodynamic information reported in literature with the Redlich-Kister equation. During the vapor pressure studies, Moser *et al.* [46] assumed that the gas consists of solely magnesium vapor. Their result of integral enthalpies of liquid Al-Mg alloys is shown in Figure 2.17. It can be observed that the calculated values for enthalpy of mixing of Al-Mg liquid alloys by Moser *et al.* [46] are similar to those of Saunders [42].

In order to establish a consistent thermodynamic description of the Mg-Al system a critical evaluation of the available thermodynamic and experimental data is needed. The reviews show a large scatter in experimental values reported for this system. In recent investigation most of the researchers adopted the thermodynamic optimization by Liang *et al.* [48]. In the current study, thermodynamic description optimized recently in COST 507 project [53] will be used to build the database for Mg-Al-Ca system. COST 507 is most recent and more accurate than [48].

2.4 Mg-Al-Ca system

2.4.1 Ternary phase diagram

Portnoi and Spektorova [54] published the information about the Mg-Al-Ca system first in 1948. They reported a pseudobinary section Mg-Al_2Ca with a eutectic liquid composition of about 79 at.% Mg. They also reported a ternary eutectic point at about 9 at.% Al and 79 at.% Mg. Dow Chemical Co. [56] confirmed the eutectic nature of the Mg-Al_2Ca section and placed the eutectic composition between 74 and 83 at.% Mg. A partial isothermal section of the Mg-rich alloys at 563K, 643K, 723K was reported by [57]. Stacey [58] recognized the possibility of a solid solution of Mg in Al_2Ca instead

of a separate ternary phase. Comparing this to other ternary systems with similar elements like Sr, the occurrence of an extended solid solution is not unlikely [8].

Gröbner *et al.* [8] investigated the phase equilibria of the Mg-Al-Ca system experimentally. They developed a thermodynamic model by incorporating all experimental data. They also determined the phase diagram in the complete composition range and reported the liquid surface for this system as shown in Figure 2.18.

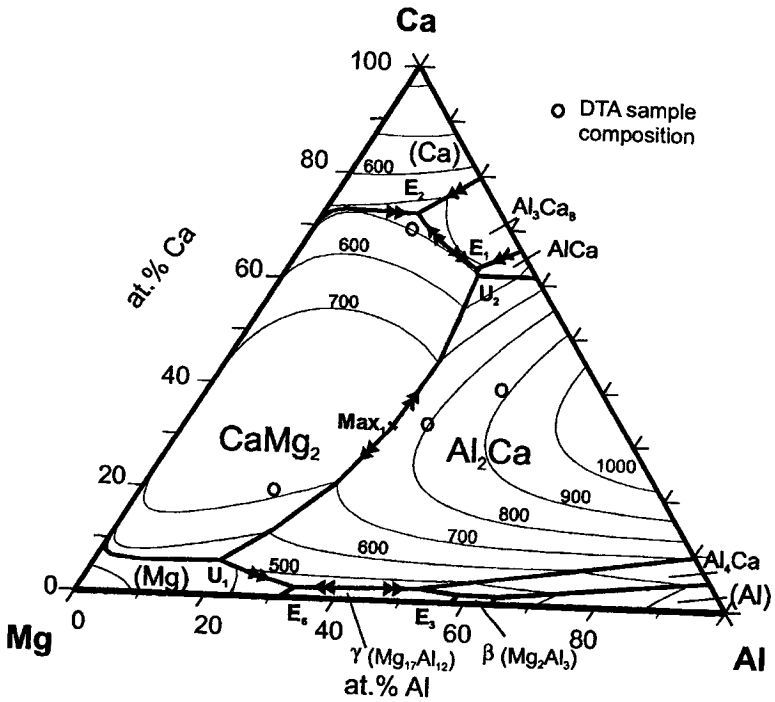

Figure 2.18: *Calculated liquidus surface with DTA sample composition [8]*

Figure 2.18 shows that the two stable Mg_2Ca and Al_2Ca are the dominating phases in this system. They [8] reported several invariant reactions in the ternary Mg-Al-Ca system. Two of the peritectic and one eutectic reactions were confirmed by experimental data. Large ternary solubilities for three binary phases Mg_2Ca, Al_2Ca and Al_3Ca_8 were found in their work. The ternary solid solubilities in Mg_2Ca–Al_2Ca section do not vary with temperature, which is reflected by the solvus lines in Figure 2.19.

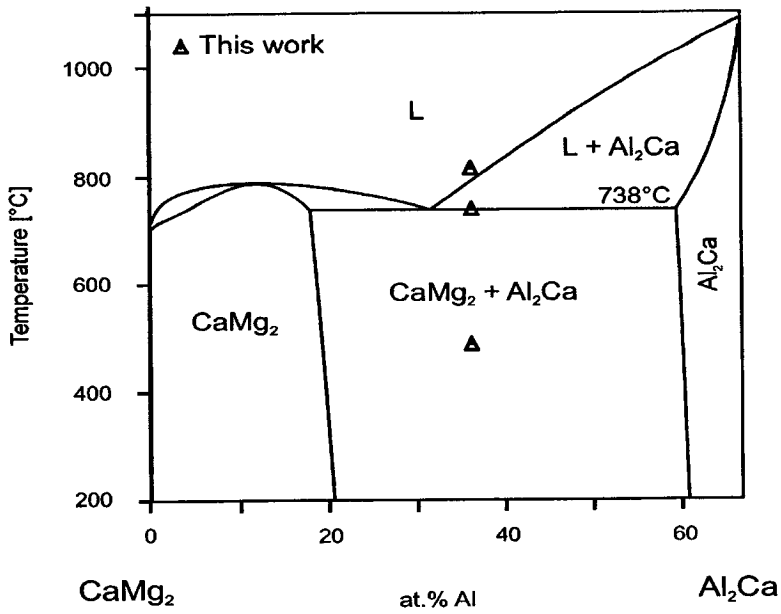

Figure 2.19: *Calculated vertical section $CaMg_2$-Al_2Ca with DTA signals from alloy Al36.67Ca33.33Mg30 [8]*

The discrepancies between the experimental work of Gröbner *et al.* [8] and the literature were observed when they worked with Ca-richer alloys. There was a strong evidence of additional binary Al-Ca phases. Therefore they performed a detailed investigation on Al-Ca system and found two new intermetallic compounds on the Ca rich side. By considering these two new intermetallic compounds they could minimize some inconsistencies in the Al-Ca system but not all.

At the same time Tkachenko *et al.* [59] published their experimental work on this system. They studied the phase equilibira in the composition range 50 to 100 wt% Mg and reported an isothermal section at 150°C, the liquidus projection on Mg-rich corner and vertical section at 4.5, 8.5 and 16 wt% Al. It was mentioned that additions of Al and Ca decrease the liquidus temperature of Mg alloys (from 650 to 438°C) and solubility of Al in Mg decreases with increasing Ca concentration in the alloys. To construct the liquidus projection, the melting point of ternary eutectic ($L_E \rightarrow (Mg) + Mg_2Ca + Al_2Ca$) at

composition 9 at.% Al, 79 at.% Mg and quasibinary eutectic ($e_3 \leftrightarrow$ (Mg) + Al_2Ca) were taken from the literature as 510°C and 535°C, respectively. Tkachenko *et al.* [59] determined another invariant point at P existing in the investigated range. This point corresponds to the peritectic transformation Lp + $Al_2Ca \leftrightarrow$ (Mg) + $Mg_{17}Al_{12}$ that occurs at 470°C as shown in Figure 2.20.

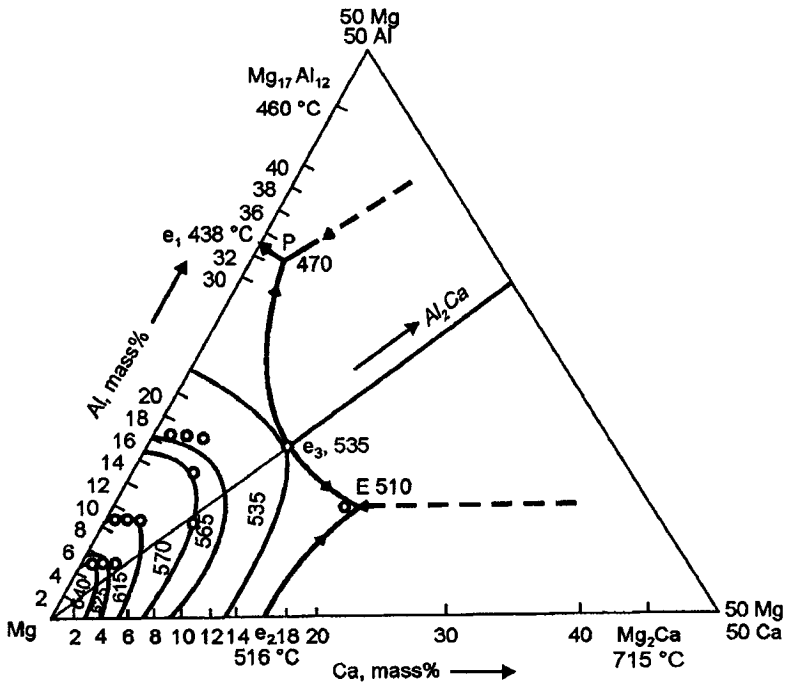

Figure 2.20: *Projection of the liquidus surface of the Mg-rich region of the Mg-Al-Ca system [59]*

Ozturk *et al.* [60] extensively studied the Mg-Al-Ca system. They calculated the ternary system to provide understanding and guidance of systematic design of Mg alloys through computational thermodynamics. They also performed experimental work for verification of calculation, refinement of thermodynamic database. For their calculation they took the thermodynamic description of the pure element from the SGTE database. They considered Liang *et al.* [48] and Agarwal *et al.* [18] work for Mg-Al and Mg-Ca system, respectively. They studied the Al-Ca system in their work to verify the existence

of two new binary phases ($Al_{14}Ca_{13}$ and Al_3Ca_8) at the Ca-rich side. During thermodynamic calculation of the Mg-Al-Ca ternary system the experimental work was still underway. Due to lack of experimental data they did not consider the solubility of the binary compounds. So, the thermodynamic description of Mg-Al-Ca ternary system was obtained by combining the data of the three binary systems. The predicted liquidus projection of the Mg-Al-Ca system is presented in Figure 2.21. It can be seen that the phase diagram is dominated by the Al_2Ca phase extensively and by the Mg_2Ca phase to some extent. These are the highest melting point compounds. They also calculated five isothermal sections at 298K, 563K, 643K, 673K and 723K. There was a good agreement between the experimental and calculated values except for the extent of the Mg phase field at 643K where the calculation predicted less Ca% than the measured values. This inconsistency may be due to the calcium loss during alloy preparation. They analyzed from isothermal sections that at low temperature there was γ phase along with Mg and Al_2Ca phases. But as the temperature increased, γ phase disappeared and there was only the wide region of Mg and Al_2Ca phases. The ratio of Al and Ca should be less than 2 to avoid γ phase. The complete elimination of γ phase from the Mg-Al-Ca alloys is important, because it is detrimental to the creep strength at elevated temperature.

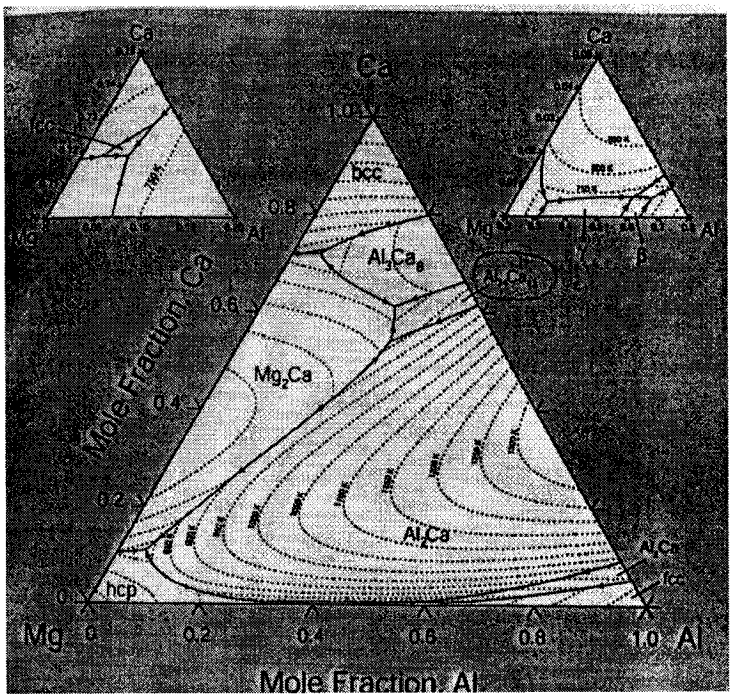

Figure 2.21: *The liquidus projection of the Mg-Al-Ca ternary system with isotherms (dotted line) [60]*

A detailed XRD and transmission electron microscopy (TEM) investigation by Luo *et al.* [4] suggested the presence of a ternary solid solution phase. It was represented by the chemical formula of $(Mg,Al)_2Ca$. This is in agreement with the result of Ozturk *et al.* [60]. In fact the metallurgical stability of the ternary $(Mg,Al)_2Ca$ phases and their interfacial coherency with the magnesium matrix were reported to be responsible for the improved creep resistance of Mg-Al-Ca alloys at temperature up to 473K. Furthermore, Al_2Ca has good mechanical properties up to 423K [9]. Al_2Ca phase was supposed to be a stable phase at both 563K and 643K, which is higher than the temperature in the automotive power train temperature. The thermal stability of both $(Mg,Al)_2Ca$ and Al_2Ca intermetallic phases can be inferred from their high melting points and eutectic temperatures. These thermally stable phases are present at the grain boundary, which prevents grain boundary sliding and improve creep resistance.

2.4.2 Thermodynamic properties

A consistent thermodynamic model was developed by [8] using the Calphad method. But no thermodynamic data are available for the liquid or the possible ternary phases.

Despite the high potential of the Mg-Al-Ca system, the complete phase diagram of this ternary system is scarcely known. There is also a question about the homogeneity range of the phases Al_2Ca and Mg_2Ca expected in the cast alloys. The liquidus projection of this system presented in the literature required further experimental verification and refinement.

CHAPTER III

The Aim of This Work

There are many opportunities for the use of magnesium alloys in the automotive drive train components because of their low density, good damping characteristics, dimensional stability, and machinability and low casting cost. Addition of Ca to Mg-Al can increase the creep and corrosion resistance as well as the strength in cast structures.

The phase diagram of ternary Mg-Al-Ca is essential for understanding the alloys' behavior and also for the determination of reactions, microstructure changes at a particular chemical composition and for further development of this system. The diagram can illustrate the phase relations and phase stability under different conditions.

Recently few studies have been committed on this system. There exist substantial discrepancies between these studies. Further refinement and verification of the ternary phase diagram is required to construct the phase relationship. In this work computational thermodynamics is applied to construct the complete ternary phase diagram of the Mg-Al-Ca system. This work has included:

- Formulation of the appropriate thermodynamic model for individual phases of the Mg-Ca and Al-Ca sub-binary systems.
- Optimization of these two systems based on experimental phase diagram and thermodynamic data available in the literature.

- Calculation of phase diagrams and thermodynamic properties for the two Mg-Ca and Al-Ca binary systems.
- Verification of the thermodynamic model by comparison with the experimental data available in the literature.
- Consideration of optimized Mg-Al system from COST 507 database. COST 507 is a multi- client research investigation concerned with the provision of a database containing critically assessed thermodynamic data for multi component light alloys [53].
- Establishing a self-consistent thermodynamic database by collecting optimized model parameters from the three binary systems.
- Calculation of isothermal sections of the Mg-Al-Ca system at different temperatures using this database
- Construction of the ternary Mg-Al-Ca phase diagram considering liquidus projections from different isothermal sections.
- Calculation of pseudobinary diagram at particular compositions to understand the behavior of a particular alloy.
- Calculation of phase assemblage diagrams for specific compositions, which help to understand the alloy behavior when changing temperature and pressure.

CHAPTER IV

Thermodynamic Modeling

4.1 Introduction

Thermodynamics deals with the transformation which energy can undergo. This study focuses on the thermodynamic modeling of the Mg-Al-Ca phase diagram. This is possible because thermodynamic properties can be deduced from phase boundaries and thermodynamics enables us to correlate diverse type of physico-chemical measurements on an alloy system and codify its properties in free energy equations [61].

Developing a thermodynamic description for an alloy system means developing appropriate thermodynamic models for all the phases in the system, so that one can calculate their equilibria and thermodynamic properties. Such a description is important not only for basic material research in related areas, such as solidification and solid-state phase transformation, but also for alloy development and improvement [62].

A phase diagram is a graphical representation of the values of thermodynamic variables when equilibrium is established among phases of a system. In recent years a quantitative coupling of thermodynamics and phase diagram is possible. With the use of computers, simultaneous optimization of thermodynamic and phase equilibria data can be applied to critical evaluation of binary and ternary systems. This approach often enables good estimations of the thermodynamic properties and phase diagrams of multi-component system. These estimates are based on structural models of solutions. The

equilibrium diagram is always calculated by minimization of the Gibbs energy. General computer programs are available for the minimization of Gibbs free energy in systems of any number of phases, components, and species [63].

The state of a two-component material at constant pressure can be presented in the well-known graphical form of binary phase diagrams as functions of temperature and composition. For three-component materials an additional dimension is necessary for a complete representation. Therefore, ternary systems are usually presented by a series of isothermal sections or projections using Gibbs triangle to represent compositions and invariant points. For systems with more than three components the graphical representation of the phase diagram is not only a challenging task but is also hindered by the lack of sufficient experimental information. However, the difficulty of graphically representing systems with many components is irrelevant for the calculation of phase equilibria [61].

J. W. Gibbs established the correlation between thermodynamics and phase equilibria more than a century ago. Hertz [64] summarized the groundbreaking work of Gibbs. It is now universally recognized that Gibbs invented a new science, that we call "Chemical Thermodynamics", when he published his three papers in the Transactions of the Connecticut Academy. At first two papers were published in 1873 and first part of third paper published in 1876 and second part in 1878. However, it took many years for this work to be discovered and its full implication to be appreciated. This delay may have been partially due to the mathematical form of this work and also may be due to the fact that the Transactions of the Connecticut Academy did not have a large international

readership, particularly in Europe. The method used by Gibbs was always mathematical modeling, which gives his work a degree of universality [65].

Over thirty-four years ago Kaufman and Bernstein [66] pioneered the thermodynamic modeling through computational coupling of thermochemic and phase equilibrium data. This approach has not only extended the horizon of classical thermodynamics but also created the foundation for today's system design of technologically important materials. They summarized the general features of the calculation of phase diagrams and also gave listings of computer programs for the calculation of binary and ternary phase diagrams, thus laying the foundation for the CALPHAD method (CALcualtion of PHAse Diagram). The CALPHAD method is based on the minimization of the free energy of the system [61].

Experimental determination of phase diagrams is a time-consuming and costly task. This becomes more pronounced when the number of components of a system increases. The advantage of the optimized phase diagrams compared with purely experimental are as follows [61, 67]:

1. The calculation of phase diagrams reduces the effort required to determine equilibrium conditions of multi-component system and focuses experimental work on critical regions.
2. A preliminary phase diagram of a higher order system can be obtained from extrapolation of the thermodynamic functions of constituent subsystems. In such case the phase diagram can be approximated with fewer experimental data.
3. This preliminary diagram can be used to identify composition and temperature with limited experimental effort.

4. Thermodynamically optimized phase diagrams are consistent as far as possible with all measured values. Consequently they are more reliable.
5. The analytical description and the optimized adjustable coefficients are convenient for storage in computer database and are easy for use.

The most reliable phase diagrams are developed when all experimental data are taken into account and if thermodynamic consistency exists between all thermodynamic functions of the different phases and the phase diagram. If these functions are presented analytically they can be extrapolated for systems with one additional component. If the analytical presentation always uses the same formalisms, all the information can be contained in a set of coefficients and is, therefore, easily stored [68].

Equilibrium is best described in terms of free energy. Gibbs free energy is a measure of a systems internal energy, which gives an indication of the randomness or entropy of the system [69]. Gibbs energy of a system is defined in terms of its enthalpy, H, entropy, S and temperature, T as:

$$G = H - TS \qquad (4.1)$$

A system at constant temperature and pressure will approach an equilibrium state that minimizes G.

The absolute values of the thermodynamic quantities are usually not known, but the changes in these quantities can be determined, by using the following expression:

$$\Delta G = \Delta H - T\Delta S \qquad (4.2)$$

Where the change in Gibbs energy of the system can be related to changes in enthalpy and entropy.

In order to determine the Gibbs energy change for the reaction at some other temperature, the following equations are used:

$$H = H_{298}^{0} + \int_{298}^{T} C_P dT \qquad \text{J/mol} \qquad (4.3)$$

$$S = S_{298}^{0} + \int_{298}^{T} \frac{C_P}{T} dT \qquad \text{J/mol.K} \qquad (4.4)$$

Therefore, it is necessary to know the heat capacity as a function of temperature for each of the reactants and products in order to calculate the changes in the enthalpy and entropy. This is usually given by an empirical series, equation 4.5 in which two to three terms generally suffice

$$C_P = a + bT + cT^{-2} + dT^{-1/2} + eT^{-3} + fT^{2} \qquad (4.5)$$

4.2 Theory

For the calculation of phase equilibria in a multi-component system, it is necessary to minimize the total Gibbs energy, G, of all the phases that take part in this equilibrium where n_i is the number of moles of phase i, G_i is the Gibbs energy of phase i and m is the number of phases.

$$G = \sum_{i=1}^{m} n_i G_i \qquad (4.6)$$

The thermodynamic models used for different phases in this work are described bellow:

4.2.1 Unary phases

The Gibbs energy of the pure element, i, with a certain phase ϕ, is described as a function of temperature by the following equations:

$$^{0}G_i^{\phi}(T) = G_i^{\phi}(T) - H_i^{SER} \quad (4.7)$$

$$^{0}G_i^{\phi}(T) = a + bT + CT\ln T + dT^2 + eT^3 + fT^{-1} + gT^7 + hT^9 \quad (4.8)$$

Where H_i^{SER} is the molar enthalpy of the stable element reference (SER) at 298.15K and 1bar, and T is the absolute temperature. The value of the coefficient a to h are taken from the Scientific Group Thermodata Europe (SGTE) compilation by Dinsdale [70].

4.2.2 Disordered solution phases

The Gibbs energy of a disordered solution phase is described by the following equation:

$$G = x_i\,{}^{0}G_i^{\phi} + x_j\,{}^{0}G_j^{\phi} + RT[x_i \ln x_i + x_j \ln x_j] + {}^{ex}G^{\phi} \quad (4.9)$$

where Φ denotes the phase in question and x_i, x_j denote the mole fraction of component i and j respectively. The first two terms on the right hand side of equation (4.9) represent the Gibbs energy of the mechanical mixture of the components, the third term is the ideal Gibbs energy of mixing, and the fourth term is the excess Gibbs energy. The excess Gibbs energy is represented using the Redlich-Kister equation:

$$^{ex}G^{\phi} = x_i.x_j \sum_{n=0}^{n=m} {}^{n}L_{i,j}^{\phi}(x_i - x_j)^n \qquad (4.10)$$

with $\quad {}^{n}L_{i,j}^{\phi} = a_n + b_n \times T \quad (n = 0,....m) \qquad (4.11)$

Where ${}^{n}L_{i,j}^{\phi}$ is the co-efficient or interaction parameters and a_n and b_n are model parameters to be optimized in terms of experimental and thermodynamic data. If the first term a_n is non-zero and the second term b_nT become very small (i.e. $|b_nT|<|a_n|$), then ${}^{n}L_{i,j}^{\phi}$ is constant and the solution is termed "regular".

The coefficient ${}^{n}L_{i,j}^{\phi}$ may be written as linear functions of temperature, T:

$$^{n}L_{i,j}^{\phi} = {}^{n}h_{i,j} - T^{n}S_{i,j} \qquad (4.12)$$

Hence the integral molar enthalpy of mixing and excess entropy of mixing, assumed independent of temperature, are given in terms of the coefficient ${}^{n}h_{i,j}$ and ${}^{n}S_{i,j}$ as:

$$\Delta h = \sum_{n=0}^{n=m} {}^{n}h_{i,j} x_i {}^{n}(1-x_i)^n \qquad (4.13)$$

$$\Delta S^E = \sum_{n=0}^{n=m} {}^{n}S_{i,j} x_i {}^{n}(1-x_i)^n \qquad (4.14)$$

where *m* is the total number of co-efficients [71]. Although other polynomials have been used in the past, in most cases they can be converted to Redlich-Kister polynomial. The advantages to the use of the Redlich-Kister expansion is, it decreases the correlation among coefficients since now the terms $(x_i - x_j)$ in equation (4.10) are zero at $x_i = x_j = 0.5$ and the terms do not all have their maximum absolute values at the same composition. Hence, with a Redlich-Kister expansion, the coefficients do not become so large so rapidly and the values are less dependent upon the total number of terms used in the series [72].

4.2.3 Stoichiometric phases

The Gibbs energy for stoichiometric compounds is described by the following equation:

$$G^{\phi} = x_i {}^0G_i^{\phi_1} + x_j {}^0G_j^{\phi_2} + \Delta G_f \qquad (4.15)$$

$$\Delta G_f = \mathrm{a} + \mathrm{b.T} \qquad (4.16)$$

where x_i, x_j are the mole fraction of component i and j and ${}^0G_i^{\phi_1}$, ${}^0G_i^{\phi_1}$ represent the Gibbs energy of a component in its standard state. However the Gibbs energy of the compound phase may refer to a different crystal structures from those of the pure elements, Φ_1 and Φ_2. ΔG_f is the Gibbs energy of formation per mole of atoms of the stoichiometric compound; the parameters a and b are obtained by optimization of the phase equilibria and thermodynamic data.

Once the binary sub-systems have been analyzed by a coupled thermodynamic/ phase diagram analysis, the phase diagram of a ternary or higher order system can usually be developed with reasonable validity. Hence, in order to minimize the experimental work, one should concentrate on re-measuring regions of the binary diagrams where required. The ternaries and quaternaries can then be recalculated as summarized in Figure 4.1 [61].

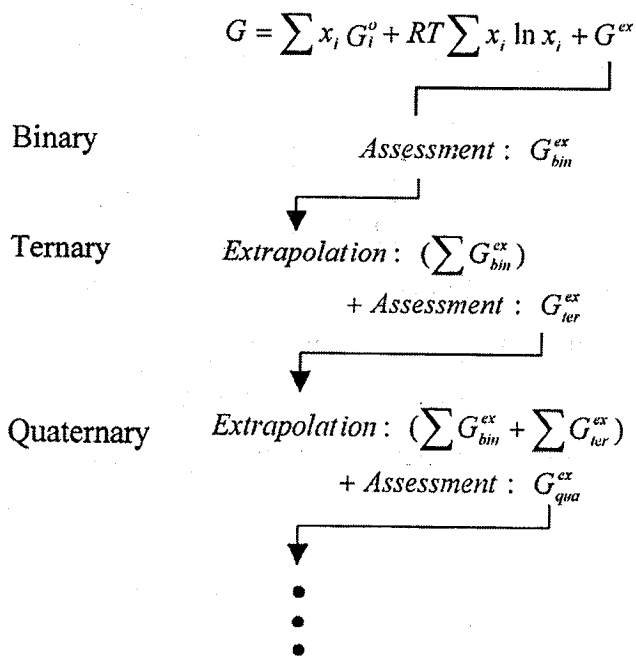

Figure 4.1: *The assessed excess Gibbs energies of the constituent subsystems are for extrapolation to a higher component system [61]*

4.3 Methodology

The storage, retrieval and manipulation of thermodynamic data with the aid of the computer require accurate analytical representation of thermodynamic properties of different phases in the system under question. Values of the standard Gibbs energies, G^{o}, of each component are collected from the SGTE database and stored in the thermodynamic database along with parameters which define the excess Gibbs energy according to the Relich-Kister polynomial model and Gibbs energy of formation of the stoichiometric compounds. In the present treatment the ternary excess Gibbs energy was calculated solely from a binary data interpretation. The ternary phase diagram was calculated by taking all the thermodynamic data stated for the binary phases into consideration. This includes the experimental phase diagrams, activity measurements and

heat and entropy of mixing. The thermodynamic and phase diagram data were critically assessed for all phases in the Mg-Ca and Al-Ca systems from room temperature to above the liquidus temperatures at the atmospheric pressure. All these data were optimized to obtain a set of model parameters for the Gibbs energy of the liquid and all solid phases as a function of composition and temperature. The model parameters are collected in a thermodynamic database. Binary phase diagrams and thermodynamic properties were calculated using this database and compared with the results from the literature. From the extrapolation of the three constituents binaries, isothermal sections of ternary system were calculated. By taking liquidus projections from these isothermal sections, a ternary phase diagram is constructed. All optimization, phase diagram and thermodynamic properties calculations of binary systems were performed by WinPhad software [73]. The enthalpy and entropy of formation of stochiometric compounds of binaries and the phase diagram of ternary system were calculated with the aid of FactSage software [74].

4.4 Construction of binary phase diagram

A system is at equilibrium when its free energy is minimum. If we could calculate the free energy of all the possible phases of a system at a specified temperature as a function of composition, it would be a simple matter to select that phase or combination of phases, which provides the lowest value of free energy for the system. By definition these would be the equilibrium phases for the system at that temperature. By repetition of these calculations for the number of temperatures, the phase boundaries of the system could be determined and the phase diagram could be constructed [75].

Determination of the phase boundaries between liquid, solid and two-phase regions in the binary diagrams is performed by constructing common tangents on the Gibbs free energy curves at temperature at which the solid and liquid phases coexist. Common tangent construction can be carried out graphically. But for the sake of higher accuracy this construction is carried out numerically. For a system with a eutectic-type diagram, the free energy-composition curves for solid solutions, α and β and for liquid solution L, at temperatures T_1, T_2, T_3, T_4, T_5 and T_6 are shown in Figure 4.2, with T_1 being the lowest and T_6 being the highest temperatures. Also shown how the information obtained in six different temperatures is combined into a single diagram to get the overall phase diagram (Figure 4.2g)

T_6, the melting point of pure A, is the first temperature at which a solid phase appears from liquid. At this temperature both α and liquid have the same free energy ($g_l = g_\alpha$) and are obviously at equilibrium. In this case the liquid phase is more stable for the entire composition range because its free energy is lower than those of other two solid phases. This stability of liquid phase (at T_6), when transferred to Figure 4.2g, shows that at T_6 isotherm only at point *a* the liquid-to-solid transition takes place and remains liquid for the whole of $0 < X_B \leq 1$ range.

At temperature T_5, the melting point of B, β and liquid L are in equilibrium with same free energy – they meet at point *b*. Moreover, α and L curves have a common tangent through points *c* and *d* (Figure 4.2e). Solid solutions of B in A with α crystal structure exist to the left of point *c*. The lowest free energy lies along the common tangent between *c* and *d*. That means liquid with composition at point *d* and α with composition at point *c* coexist in this interval. The liquid L is more stable throughout to

the right of composition at *d* with lower Gibbs energy than that of other phases. Carrying over this information to Figure 4.2g shows three points *c*, *d* and *b* on T_5 isotherm.

At next lower temperature T_4, two different common tangents can be drawn – one between α and liquid phases at compositions *e* and *f*, and the other between liquid and β phases at compositions *g* and *h*. Translating this into Figure 4.2g shows that both α + liquid and β + liquid two phase zones are present at temperature T_4.

Figure 4.2c shows that all three phases (α, β and L) have a common tangent, thus a unique temperature. Transferring this information to Figure 4.2g gives three points *j*, *k* and *l* on the isotherm line of T_3 showing that the three phases coexist at this temperature. This is the *eutectic point* of the system – it corresponds to the lowest temperature below which no liquid can exist.

At lower temperatures (T_1 and T_2), α and β phases coexist between m and n (Figure 4.2b) and between o and p (Figure 4.2a) compositions – this results in the area *o-m-j-k-l-n-p* (Figure 4.2g) for the two-phase region. Beyond this region only single phases (α at A-rich zone β at B-rich zone) exist.

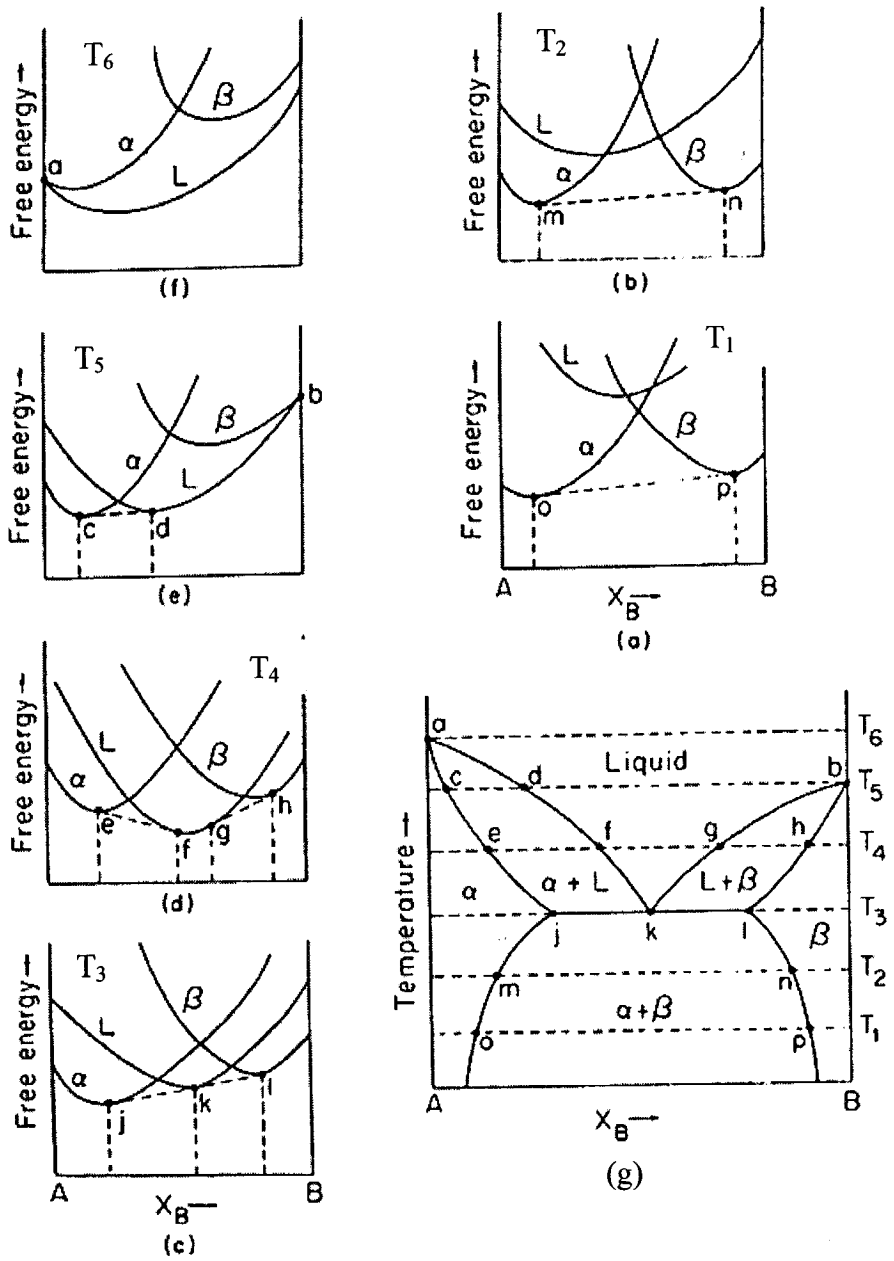

Figure 4.2: *(a)-(f) Free energy-composition curves at T_1-T_6, respectively, and the temperature- true-composition diagram for a eutectic system, 4.2(g) shows the overall phase diagram derived from (a)-(f) [76].*

In the above example with Figure 4.2, phase diagram construction for only simple binary eutectic system is shown. Now the phase diagram construction will be extended for system with intermediate phases.

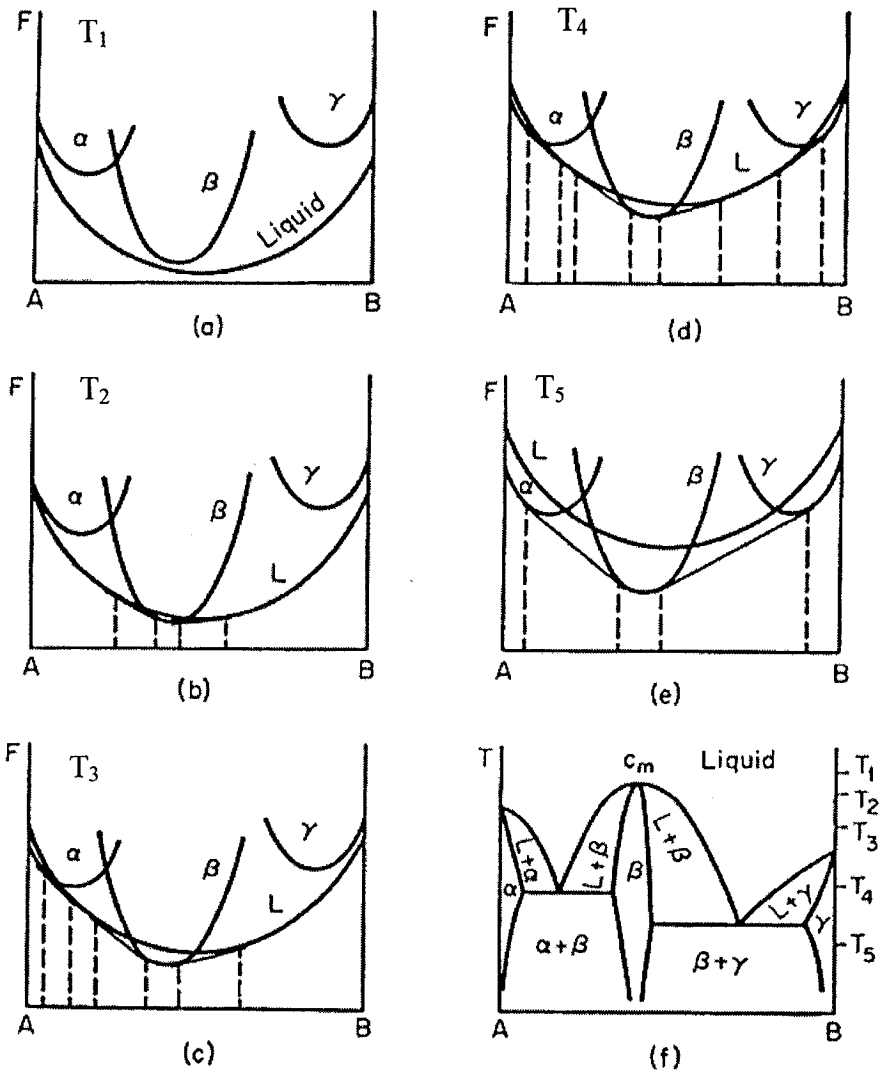

Figure 4.3: *(a)-(e) Form of equilibrium diagram at T_1-T_5, respectively, in which an intermediate phase forms directly from the liquid, (f) shows the overall diagram [78].*

A system containing intermediate phases is shown in Figure 4.3. The free energy curves for different phases at different temperatures are also shown. At temperature T_1 the liquid phase has the lowest free energy over the entire composition range. Thus this is the most stable phase at this temperature. At T_2, however, the free energy curve of liquid crosses that of the intermediate phase, β, and the free energy curves of primary solutions α and γ are still too high. At lower temperatures T_3 and T_4, the free energy curves of

liquid phase are intersected not only by that of the intermediate phase, β, but also by those of α and γ phases. Two eutectics are formed between the intermediate phase and each of the terminal phases. The general feature of all systems in which an intermediate phase forms directly from the liquid is a maximum in the solidus and liquidus curves where the phase is formed. The composition at the maximum, $C_{m,}$ corresponds also to the composition at which the minimum occurs in the free energy curve of the intermediate phase [77].

CHAPTER V

Results and Discussions

The Mg-Al-Ca ternary system consists of three binary constituents Mg-Ca, Al-Ca and Mg-Al systems. Although several optimizations have already been done on these systems still additional work is required such as reduction of number of parameters of thermodynamic models and finding a better fit of data. Two binaries Mg-Ca, Al-Ca systems are optimized in this work. During optimization, the thermodynamic models are kept as simple as possible by reducing the number of parameters because a higher number of parameters in a binary system is not only difficult to interpret but also results in uncertainty when extrapolating to a higher order system. The optimized parameters for the Mg-Al system are taken from COST 507 database, as this is the most recent and reliable.

During optimization of phase diagram of binary systems, all available thermodynamic and phase equilibria data were critically evaluated to obtain a set of model parameters for Gibbs energy equation of all the phases as a function of composition and temperature. The optimization process was carried out using Winphad Pro 2.0 software [73]. Prior to carrying out the optimization, a careful evaluation of the experimental data reported in the literature is essential because these sets of data are not always in agreement. The Gibbs energy equation with optimized parameters can be used to calculate the phase diagrams that match the experimental ones, and can provide an assurance of global optimum values of the model parameters. An essential validation is

obtained by comparing thermodynamic properties (enthalpy, activity and Gibbs free energy) obtained through these optimum parameters with those from the literature.

Phase diagrams are forms of thermodynamic data since they present the conditions of minimum Gibbs energy of a system in terms of phases present for a given overall composition, temperature and pressure. At a specified temperature and pressure the most stable product(s) is the one that is associated with the lowest Gibbs energy. The products of the reactions are either solution phases or stoichiometric phases. So if the existence of a particular phase does not assist in minimization of G, it will be dropped in the course of successive iterations [65].

5.1 Mg-Ca system

5.1.1 Phase diagram

The mathematical expressions for Gibbs energy of the different phases are shown in Table 5.1. The model-calculated phase diagram of the Mg-Ca system in relation with experimental results from the literature is shown in Figure 5.1. This diagram was calculated from the database built for the Mg-Al-Ca system. For instance, in the Mg-Ca system for liquid phase the reference states of both components are Ca-liquid and Mg-liquid and for the terminal solid solution phase, the reference states of both components are Ca-Hcp and Mg-Hcp. For the stoichiometric compound, the reference state of Mg and Ca are different and they are Mg-Hcp and Ca-Fcc, respectively. The Gibbs energy of components in standard state is taken from SGTE database [70].

Table 5.1: *Thermodynamic model for the phases in Mg-Ca system.*

Phase Name	Input data [70]	Gibbs energy equation
Liquid	${}^{\circ}G_{Ca-L}$=5844.85+62.4838T-16.3138×TlnT-0.0111T^2-133574T^{-1} ${}^{\circ}G_{Mg-L}$=-165.10+134.8390T-26.1850×TlnT-0.0005T^2+78950T^{-1}-1.3937×10^{-6}×T^3-8.0176×10^{-20}×T^7	$G=X_{Ca}{}^{\circ}G_{Ca-L}+X_{Mg}{}^{\circ}G_{Mg-L}+RT(X_{Ca}\ln X_{Ca}+X_{Mg}\ln X_{Mg})+X_{Ca}X_{Mg}\sum_{i=0}^{k}{}^{i}L(X_{Mg}-X_{Ca})^{i}$ ${}^{\circ}L = -24018.60 + 1.9433T$ ${}^{1}L = 1785.73 + 4.4724T$ ${}^{2}L = 14387.50 - 22.9827T$
Solid solution	${}^{\circ}G_{Ca-Hcp}$=-4455.06+73.4943T-16.3138×TlnT-0.0111T^2-133574T^{-1} ${}^{\circ}G_{Mg-Hcp}$=-8367.34+143.6760T-26.1850×TlnT-0.0005T^2+78950T^{-1}-1.3937×10^{-6}×T^3	$G=X_{Ca}{}^{\circ}G_{Ca-Hcp}+X_{Mg}{}^{\circ}G_{Mg-Hcp}+RT(X_{Ca}\ln X_{Ca}+X_{Mg}\ln X_{Mg})+X_{Ca}X_{Mg}\sum_{i=0}^{k}{}^{i}L(X_{Ca}-X_{Mg})^{i}$ ${}^{\circ}L = 7150.90 - 9.4013T$
Stoichiometric Compound	${}^{\circ}G_{Ca-Fcc}$=-4955.06+72.7943T-16.3138×TlnT-0.0111T^2-133574T^{-1} ${}^{\circ}G_{Mg-Hcp}$=-8367.34+143.6760T-26.1850×TlnT-0.0005T^2+78950T^{-1}-1.3937×10^{-6}×T^3	$G=X_{Ca}{}^{\circ}G_{Ca-Fcc}+X_{Mg}{}^{\circ}G_{Mg-Hcp}+\Delta G_{f-Mg2Ca}$ $\Delta G_{f-Mg2Ca} = -12704.40 + 1.8094T$

It can be seen from Figure 5.1 that there is a good agreement between experimental and calculated results. In the Ca-rich region this calculated phase equilibria data agree fairly well with the results from the literature. The calculated eutectic composition and temperature agree very well with the experimental values from literature. This indicates that the polynomial representation of the solution phases is capable of reproducing the measured phase diagram within experimental error limits, even when the measurements are very precise.

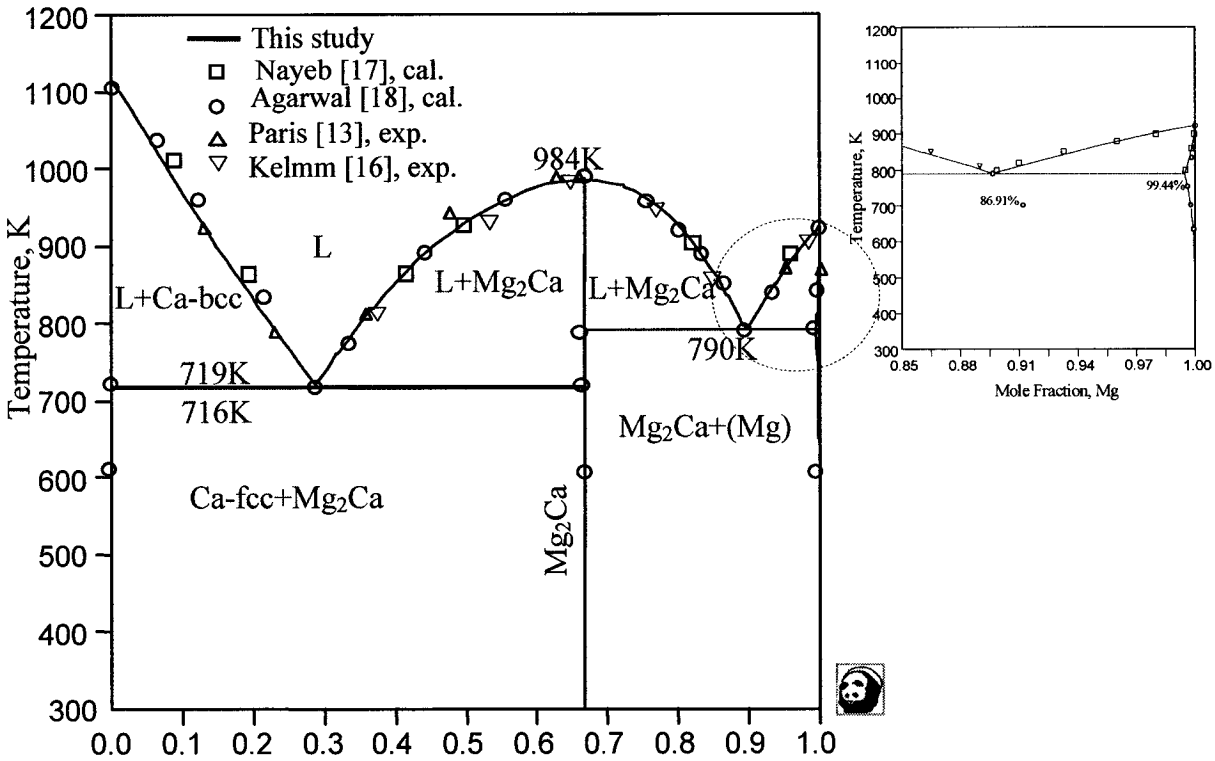

***Figure 5.1**: Optimized Mg-Ca with experimental data from the literature (cal: calculated, exp: experimental)*

The melting point of pure Mg (923K) reported by Agarwal *et al.* [18] agrees well with the value resulting from the present model, 923K. However Nayeb-Hashemi and Clark [17] reported the melting point of Mg as 878K. Also, the calculated melting point of pure Ca, 1115K, reported by [18] and [17] is the same value that resulted from the present model. The transition temperature from α-Ca (fcc) to β-Ca (bcc) 716K, was reported by [18] and [17]. The current model reproduces this value. Agarwal *et al.* [18] and Nayeb-Hashemi and Clark [17] reported the eutectic composition and temperature on Ca-rich side as 28.6% Mg at 719K and 27%Mg at 718K, respectively and on Mg-rich side as 89.5%Mg at 790K and 89.5% at 789.50K, respectively. Comparing these results with the corresponding eutectic points on the Ca and Mg-rich sides in Figure 5.1, 28.83%Mg at

719K and 89.61%Mg at 790K, respectively, indicates good agreement. The eutectic reactions, which occur on the Ca and Mg-rich sides, are $L \rightarrow Mg_2Ca+\alpha Ca$ and $L \rightarrow Mg_2Ca+Mg$, respectively.

There is no homogeneity field for Mg_2Ca compound. [18] and [17] reported the melting point of Mg_2Ca as 984K and 988K, respectively, which is in good agreement with the value found in the present work at 984K.

There is a small solubility range of Ca in Mg. The (Mg) solidus can be represented by an almost straight line originating from the melting point of Mg and terminating at 99.44%Mg at 790K as shown in Figure 5.1. This is in good agreement with the results of [18] and [17].

5.1.2 Thermodynamic properties

This section illustrates the calculated results of thermodynamic properties (enthalpy, activity etc.) of Mg-Ca system. The calculated values are compared with the experimental results available in literature.

Thermodynamic data for the liquid and the Mg_2Ca intermetalllic compound are available in the literature. In Figure 5.2 the model-calculated enthalpy of mixing shows good agreement with experimental data measured by Sommer *et al.* [24]. Although Agarwal *et al.* [18] also measured the enthalpy of mixing at 1023K, their results were not considered for the optimization because they contradict those of Sommer *et al.* [24]. However, Mishra *et al.* [25] mentioned that considering energy parameters values at 1023K instead of 1150K could minimize this discrepancy.

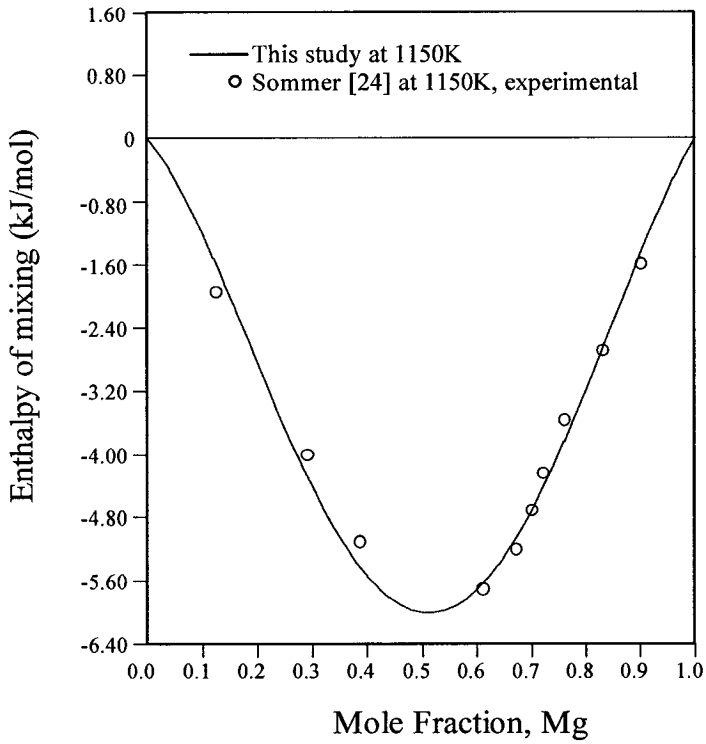

Figure 5.2: *Enthalpy of mixing Mg-Ca liquid at 1150K*

The activity of Mg in Mg-Ca liquid at 1080K is shown in Figure 5.3. It can be seen from this figure that the calculated Mg activity agrees with the experimental results from the literature. Also, the figure shows that Mg mixing in the Mg-Ca liquid demonstrates negative deviation from Raoult's ideal solution.

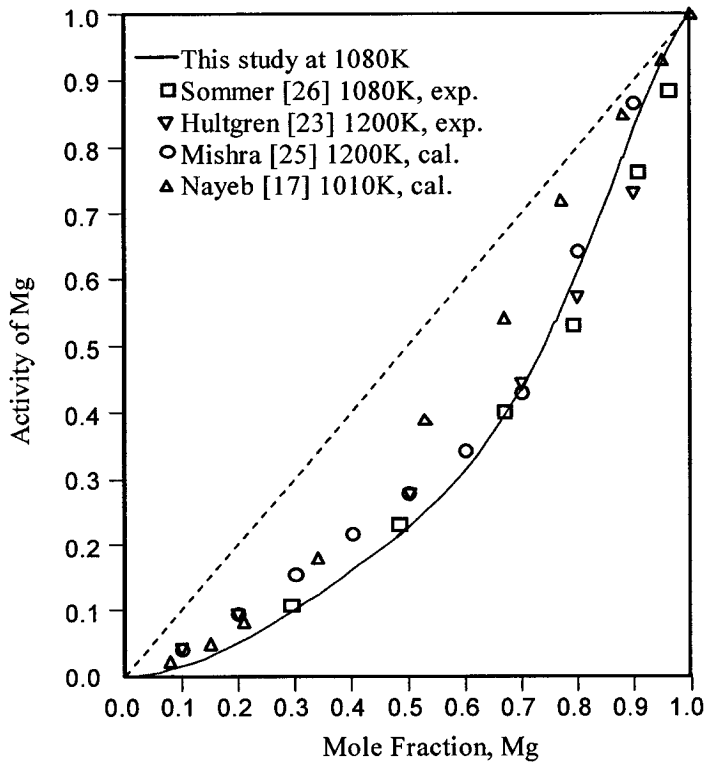

Figure 5.3: *Activity of Mg in Mg-Ca liquid (cal: calculated, exp: experimental)*

It can be seen from Figure 5.4 that the calculated activity of Ca agrees with the results obtained by Sommer [26]. However the activities of Ca reported by Hultgren *et al.* [23] and Mishra *et al.* [25] are higher than those of [26]. This is probably due to the fact that they obtained their results at a significantly different temperatures. Sommer [26] and Hultgren *et al.* [23] determined the activity of Ca experimentally and Mishra *et al.* [25] calculated it. Sommer [26] measured activities of Ca only for Ca-rich alloys. But later the activities of Ca for alloys across the phase diagram were obtained from those of Mg, using the Gibbs-Duhem equation.

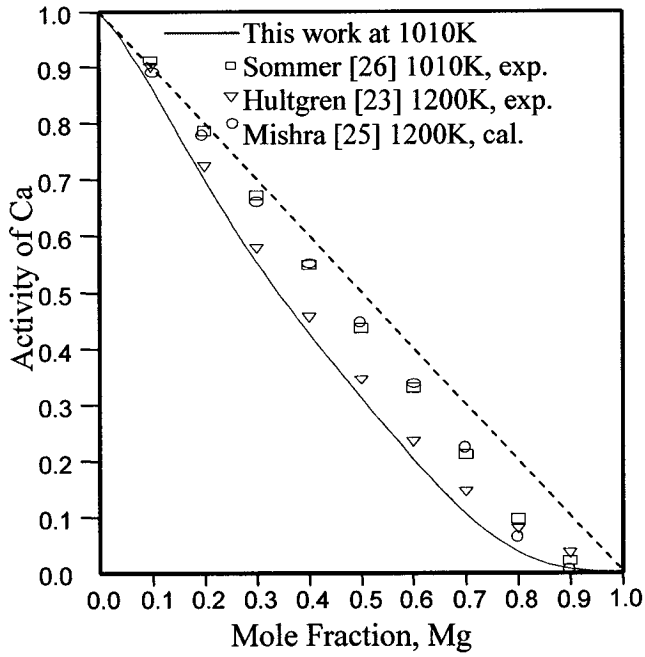

Figure 5.4: *Activity of Ca in Mg-Ca liquid (cal: calculated, exp: experimental)*

Figures 5.5 and 5.6 show that calculated partial Gibbs free energy of Mg and Ca in Mg-Ca liquid at 1100K follows the trend of the experimental data from the literature.

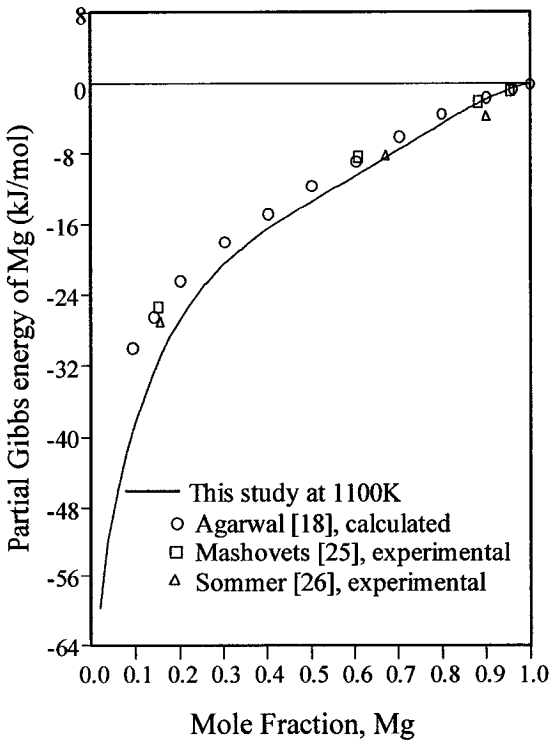

Figure 5.5: *Partial Gibbs energy of Mg in Mg-Ca liquid*

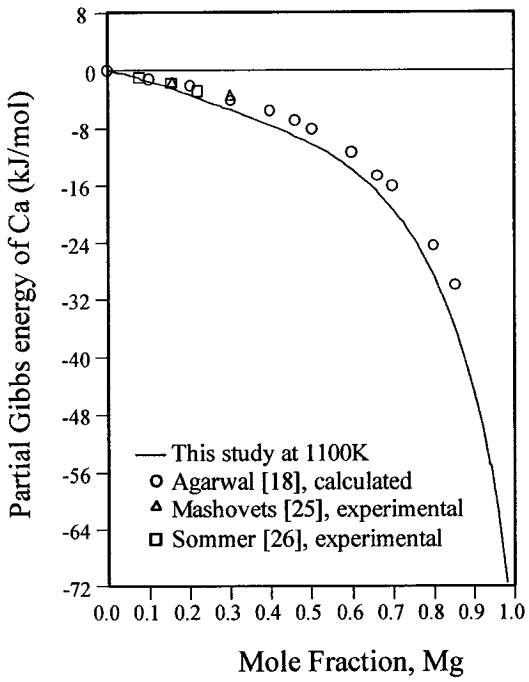

Figure 5.6: *Partial Gibbs energy of Ca in Mg-Ca liquid*

Experimental results from Agarwal *et al.* [18] for partial enthalpy of mixing of Ca in Mg-Ca liquid at 1032K are compared with calculated values in Figure 5.7.

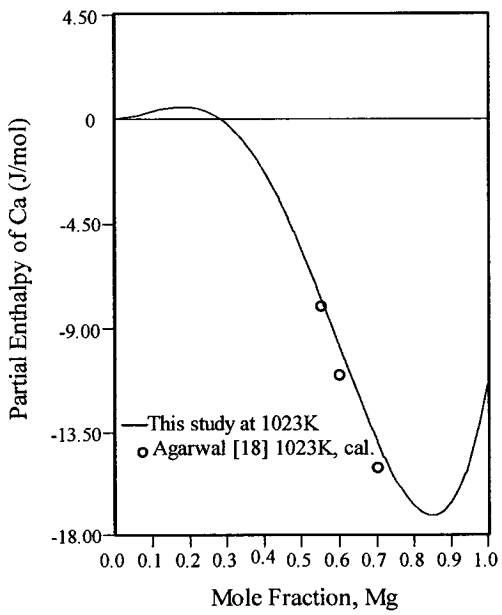

Figure 5.7: *Partial enthalpy of Ca in Mg-Ca liquid (cal: calculated)*

Although these data were predicted, i.e. they were not included in the optimization, they agree well with the results calculated from the thermodynamic model.This provides strong evidence of the quantity of the model.

In this study the calculated enthalpy and entropy of formation of Mg_2Ca stoichiometric compound at 298K is –12.70 kJ/g-atom and 1.81 J/g-atom.K, respectively. Davison and Smith [22] and King and Kleepaa [21] proposed the enthalpy of formation at 298K as –13.17 kJ/g-atom and –13.5 kJ/g-atom, respectively. Hultgren *et al.* [23] reported the entropy of formation to be –0.84 J/g-atoms.K. These are close to the values resulting from the current model.

5.2 Al-Ca system

5.2.1 Phase diagram

The optimized phase diagram of Al-Ca system in relation with experimental data from the literature is shown in Figure 5.8.

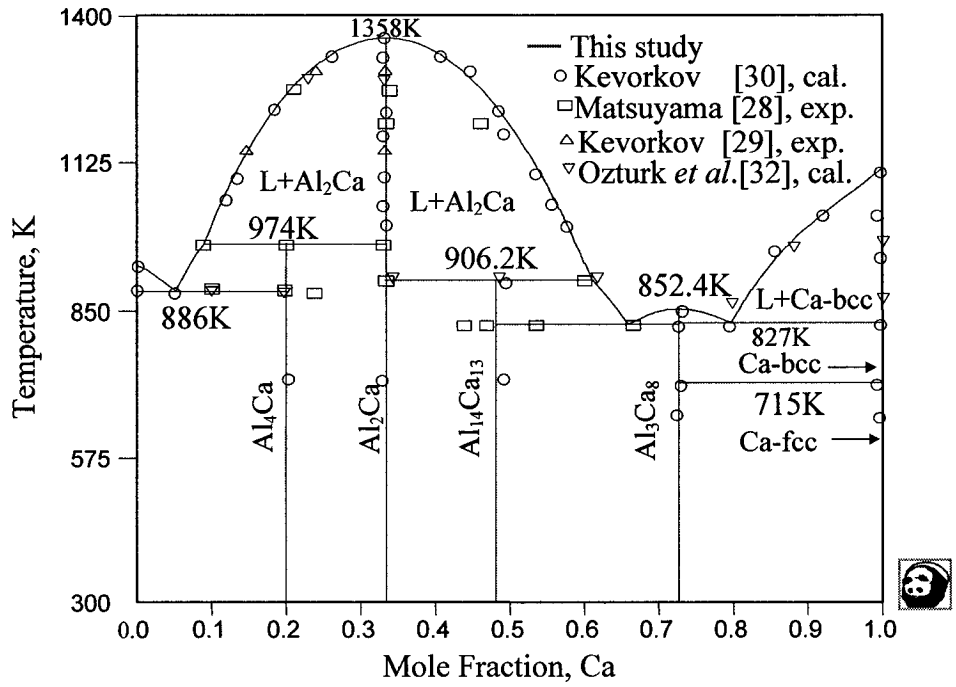

Figure 5.8: *Calculated Al-Ca phase diagram with experimental data from literature (cal: calculated, exp: experimental)*

Since two compounds in the Ca-rich side have been discovered recently, the most recent experimental results of Keverkov and Schmid-Fetzer [29, 30] for the Al-Ca system were chosen for optimization. Agreement between the model-calculated phase diagram and the measured liquidus and other critical points can be seen in this figure. Nevertheless the discrepancy between the results of Matsuyama [28] and the current work is due to the fact that he considered only two intermediate compounds Al_4Ca and Al_2Ca in this system. The melting point of pure Al-fcc, 933K, reported by Kevorkov *et al.* [30] and Ozturk *et al.* [32] is the same with the value resulted from the present model, 933K. The melting point of pure Ca, 1114.90K, reported by [30] agrees very well with the value that resulted from the present model, 1115K. The transition temperature at 715.9K, from α-Ca (fcc) to β-Ca (bcc), was reported by [30]. This is the same temperature as the one resulted from the current work. Kevorkov *et al.* [30] reported one eutectic point on Al-rich side (5.1% Ca at 886K) and two eutectic points on Ca-rich side (66.5%Ca at 825.10K and 79.5%Ca at 827.50K). Comparing these results with the corresponding eutectic points in Figure 5.8, 5.1%Al at 886K on Al-rich side and 65.97%Ca at 825K and 79.69%Ca at 828K on Ca-rich side, provides good agreement. The eutectic reaction that occurs on Al-rich side is according to: $L \rightarrow Al_4Ca + Al(fcc)$ and on Ca-rich side two eutectic reactions take place according to: $L \rightarrow Al_{14}Ca_{13} + Al_3Ca_8$ and $L \rightarrow Al_3Ca_8 + \beta Ca$.

There are four intermetallic compounds Al_4Ca, Al_2Ca, $Al_{14}Ca_{13}$ and Al_3Ca_8 in this system without any homogeneity field. The melting points of Al_4Ca, Al_2Ca and Al_3Ca_8 reported by [30] are at 974.3K, 1359.60K and 853.4K, respectively. These values are in good agreement with the results, (974K, 1358K and 852K) obtained from the present

model. The fourth compound can be either $Al_{14}Ca_{13}$ [32] or AlCa [30]. This study considers $Al_{14}Ca_{13}$ because the crystal structure of this compound is known [31]. The melting point and composition of $Al_{14}Ca_{13}$ compound reported by Ozturk *et al.* [32] are 906.50K and 48.46% Ca. Kevorkov *et al.* [30] determined the melting point and composition of AlCa as 906K and 50%Ca, respectively. The calculated melting point and composition of $Al_{14}Ca_{13}$ compound in this work are 907K and 48.14%Ca, which agree well with [32]. Moreover two peritectic points found in this study match well with the peritectic points mentioned by Kevorkov *et. al.* [30]. In their study, one peritectic point occurs at 9.8 at.% Ca and 974.30K, and the other at 61.6 at.% Ca and 906.20K whereas; the calculated values are 9.06 at.% Ca and 974K, and 61 at.% Ca and 907K, respectively. In this research, the two peritectic reactions are $L + Al_2Ca \rightarrow Al_4Ca$ taking place at 2 at.% Ca and 974K, and $L+Al_2Ca \rightarrow Al_{14}Ca_{13}$ occurring at 50 at.% Ca and 907K.

The mathematical expressions for Gibbs energy of different phases are shown in Table 5.2. For Al-Ca liquid, the reference states of both components are Al-liquid, Ca-liquid. For stoichiometric compounds the reference state of Al and Ca are Al-Fcc and Ca-Fcc, respectively. The Gibbs energy of components in standard state or reference state is taken from the SGTE database [70].

***Table 5.2**: Mathematical model of Al-Ca binary system:*

Phase Name	Input data [70]	Gibbs energy equation	
Liquid	${}^{\circ}G_{Ca-L}$=5844.85+62.4838T-16.3138×TlnT-0.0111T^2-133574T^{-1} ${}^{\circ}G_{Al-L}$=-3028.88+125.251T-24.3672×TlnT-0.0019T^2 +74092T^{-1}-8.7766×10^{-7}×T^3+7.934e-020T^7	G=X_{Ca} ${}^{\circ}G_{Ca-L}$+ X_{Al} ${}^{\circ}G_{Al-L}$+RT (X_{Ca} ln X_{Ca}+ X_{Al} ln X_{Al})+ X_{Ca} X_{Al} $\sum_{i=0}^{k} {}^{i}L(X_{Ca}-X_{Al})^{i}$ ${}^{\circ}L$ = -87894.60 + 29.8567T ${}^{1}L$ = -12077.60 + 4.8063T ${}^{2}L$ = 11427.80 – 2.4505T ${}^{3}L$ = -1058.76 – 0.9537T	
Stoichiometric Compound	${}^{\circ}G_{Ca-Fcc}$=-4955.06+72.7943T-16.3138×TlnT-0.0111T^2-133574T^{-1} ${}^{\circ}G_{Al-Fcc}$=-7976.15+137.093T-24.3672×TlnT-0.0019T^2+74092T^{-1}-8.7766×10^{-7}×T^3	G=X_{Ca} ${}^{\circ}G_{Ca-Fcc}$+ X_{Al} ${}^{\circ}G_{Al-Hcp}$+ΔG_f	
		Al_4Ca	$\Delta G_{f-Al4Ca}$= – 17272 + 2.2389T
		Al_2Ca	$\Delta G_{f-Al2Ca}$= – 29281.70 + 5.3818T
		$Al_{14}Ca_{13}$	$\Delta G_{f-Al14Ca13}$= –26058.50 + 5.6347T
		Al_3Ca_8	$\Delta G_{f-Al3Ca8}$= – 15627.30 + 2.3014T

5.2.2 Thermodynamic properties

The calculated enthalpy of mixing of Al-Ca liquid in relation with experimental results from the literature is presented in Figure 5.9. It can be seen that there is an excellent agreement between this study and Kevorkov *et al.* [30] and Notin *et al.* [35]. However this figure shows that there is a reasonable agreement with Sommer *et al.* [36]. Nevertheless, an attempt to get close fit to enthalpy of mixing measured by Sommer *et al.* [36] resulted in shifting the liquidus line of Al_2Ca to higher temperature on Ca-rich side.

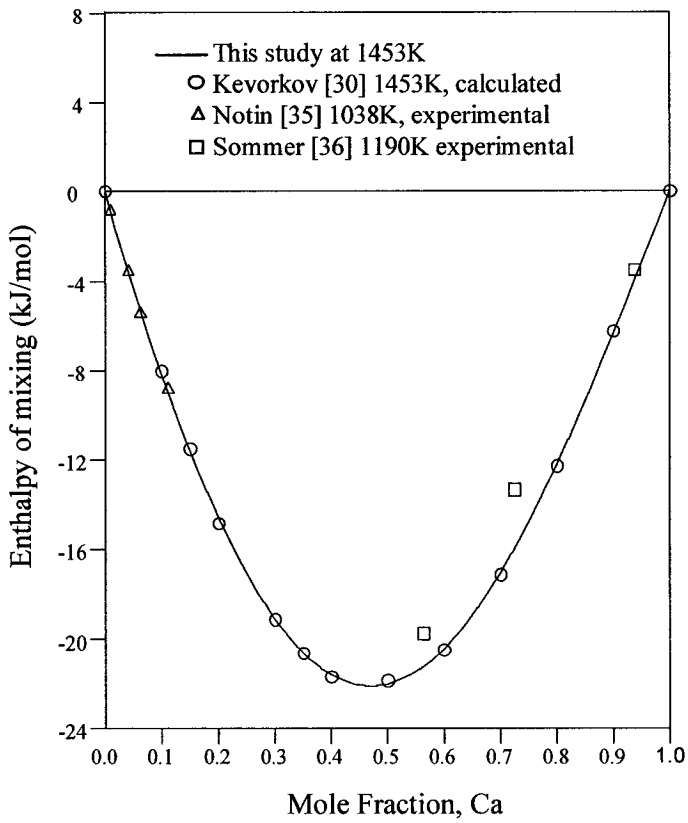

Figure 5.9: *Enthalpy of mixing of Al-Ca liquid at 1453K*

The calculated activity of Ca agrees well with the results obtained by Ozturk *et al.* [32] and Schürmann *et al.* [38] as shown in Figure 5.10. Jacob *et al.* [37] determined the thermodynamic activities at 1373K for liquid Al-Ca alloys using the Kundsen effusion method for the composition range 0 to 38 at.% Ca and a distribution method for the composition range 44 to 100 at.% Ca. The calculated activity of Al at 1373K in this work is shown in Figure 5.11. The calculated and experimental values agree fairly well. If the activity of Ca is calculated at higher temperature, it shows less negative deviation from ideal condition.

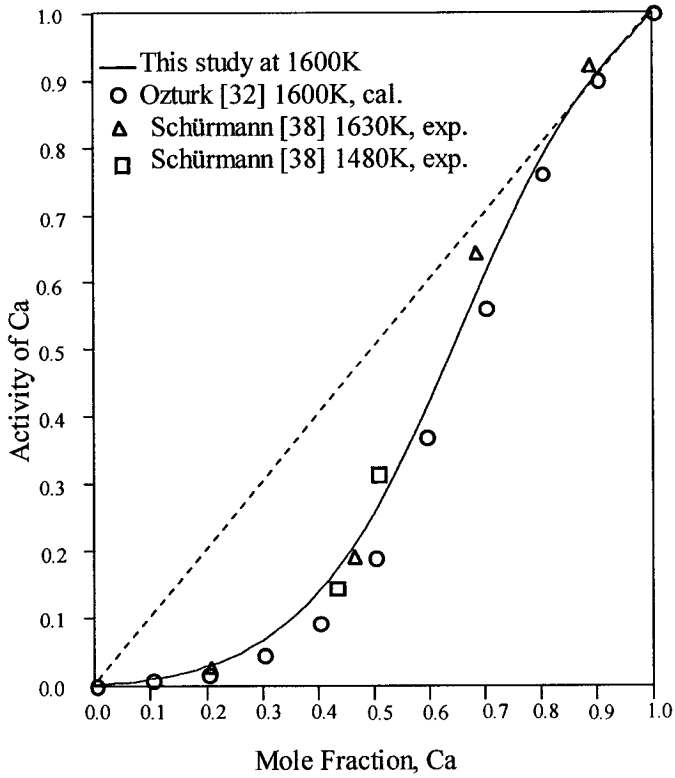

Figure 5.10: *Activity of Ca in Al-Ca liquid (cal: calculated, exp: experimental)*

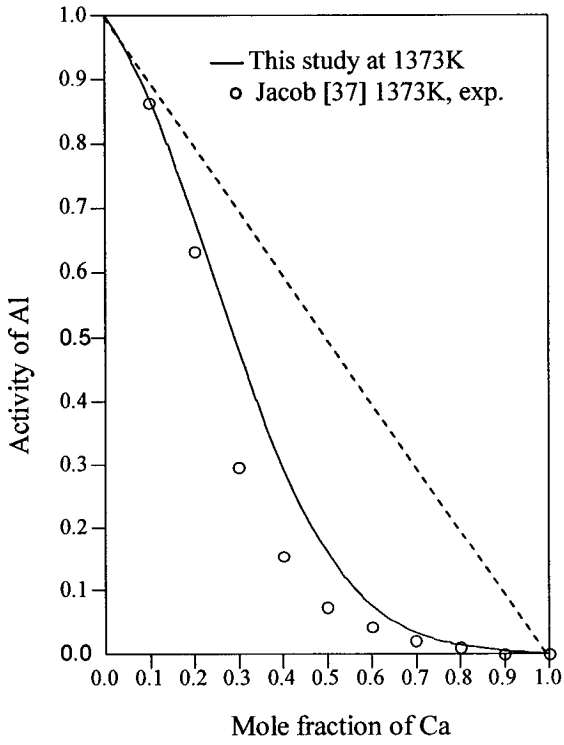

Figure 5.11: *Activity of Al in Al-Ca liquid (cal: calculated, exp: experimental)*

The calculated thermodynamic properties for the four intermetallic compounds are compared with other data from the literature in Tables 5.3 to 5.6.

The thermodynamic properties of Al_2Ca are listed with data from the literature in Table 5.3. It can be seen that the enthalpy, entropy and Gibbs energy of formation of Al_2Ca obtained in this study agree with the results from the literature.

Table 5.3: *Thermodynamic properties of Al_2Ca with experimental data from the literature.*

Method [Ref]	**T(K)**	**$\Delta_f H$ kJ/g-atom**	**$\Delta_f S$ J/g-atom.K**	**$\Delta_f G$ kJ/g-atom**
PC [35]	1038	-33.40±0.60		
Emf [39]	800	-34.30±3.50	-6.10±1.10	-28.30±0.30
DC [30]	298	-29.40±0.90		
A [30]	800	-29.70	-5.02	-25.70
Cal*	298	-29.28	-5.38	-27.70

PC: Precipitation Calorimetry, DC: Dissolution Calorimetry A: Assessed, Cal*: Calculated from this work.

The thermodynamic properties of Al_4Ca are listed with data from the literature in Table 5.4. The values obtained in this work agree with the results from the literature. Further, the calculated Gibbs energy of formation of this compound is similar to the assessed value of Kevorkov *et al.* [30].

Table 5.4: *Thermodynamic properties of Al_4Ca with experimental data from the literature.*

Method [Ref]	**T(K)**	**$\Delta_f H$ kJ/ g-atom**	**$\Delta_f S$ J/ g-atom.K**	**$\Delta_f G$ kJ/ g-atom**
PC [35]	1038	-18.70 ±0.30		
Emf [39]	800	-19.40 ±3.30	-1.10±0.50	-17.80±0.14
A [30]	800	-21.00	-5.49	-16.60
Cal*	298	-17.27	-2.24	-16.60

PC: Precipitation Calorimetry, A: Assessed, Cal*: Calculated from this work.

The existence of two intermetallic compounds Al_3Ca_8 and $Al_{14}Ca_{13}$ is indicated in most recent studies [29,31]. So, few experimental values for their thermodynamic properties are reported in the literature. Table 5.5 lists the thermodynamic properties of Al_3Ca_8 in comparison with data from the literature. It can be seen that the enthalpy and Gibbs energy of formation of this compound agree with the results from the literature.

Table 5.5: *Thermodynamic properties of Al_3Ca_8 with experimental data from the literature.*

Method [Ref]	**T(K)**	**$\Delta_f H$ kJ/ g-atom**	**$\Delta_f S$ J/ g-atom.K**	**$\Delta_f G$ kJ/ g-atom**
DC[30]	298	-13.70±1.30		
A [30]	800	-14.00	-0.47	-13.60
Cal*	298	-15.63	-2.30	-14.94

DC: Dissolution Calorimetry, A: Assessed, Cal*: Calculated from this work.

The thermodynamic properties for $Al_{14}Ca_{13}$ are not available in the literature yet. Hence the calculated thermodynamic properties for this compound are compared with the properties of AlCa in Table 5.6. It was noticed that the thermodynamic properties of these two compounds are very close.

Table 5.6: *Thermodynamic properties of $Al_{14}Ca_{13}$*

Method [Ref]	**T(K)**	**$\Delta_f H$ kJ/ g-atom**	**$\Delta_f S$ J/ g-atom.K**	**$\Delta_f G$ kJ/ g-atom**
Cal*$Al_{14}Ca_{13}$	298	-26.06	-5.63	-24.38
A [30] AlCa	800	-22.80	-2.15	-21.10

Cal*: Calculated from this work, A: Assessed.

The calculated and experimental values of enthalpy of formation of the four stoichiometric compounds are shown in Figure 5.12.

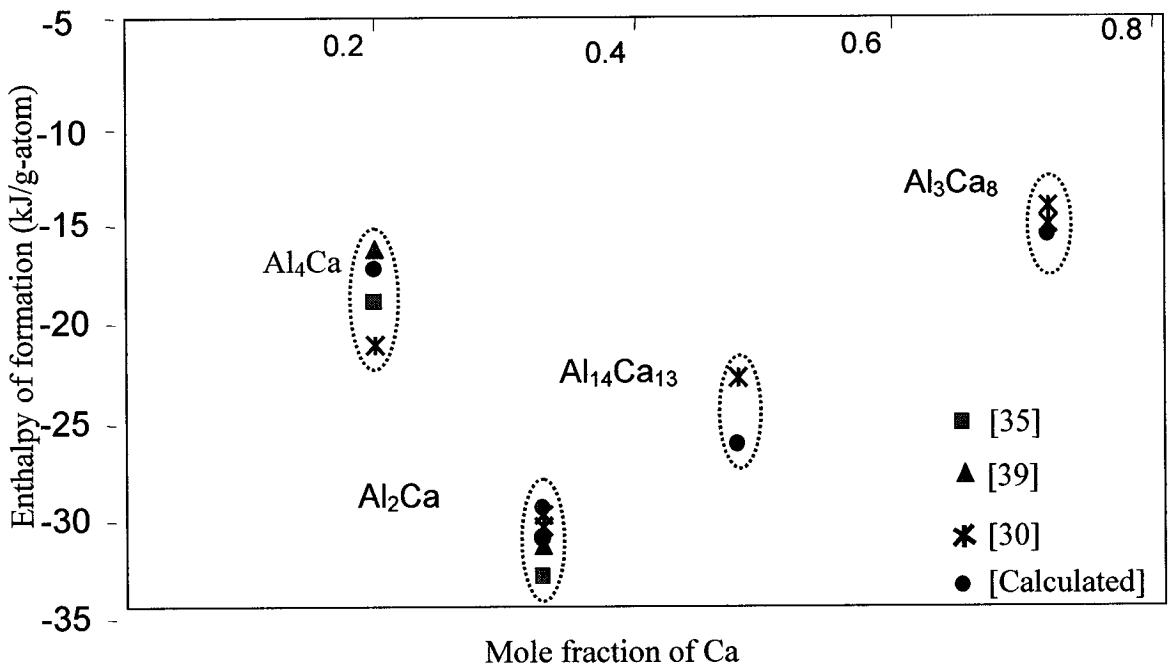

Figure 5.12: *Enthalpy of formation of different stoichiometric compound in Al-Ca system*

Results from the four previous studies and the current research are plotted in Figure 5.12, which shows four clusters of data-points for four different compounds. It can be seen that the results obtained in this study agree with those from the literature. The difference obtained for $Al_{14}Ca_{13}$ may be due to the fact that Kevorkov *et al.* [30] considered this compound as AlCa, as discussed earlier.

5.3 Mg-Al-Ca systems

5.3.1 Isothermal Sections

Isothermal sections are directly calculated from the database developed by this study for the Mg-Al-Ca system. The ternary phase diagrams were calculated by assuming the ternary parameters to be zero, and taking all the thermodynamic data stated for the binary phases into consideration. The calculated isothermal sections of the Mg-Ca-Al system are given in Figures 5.13 to 5.17.

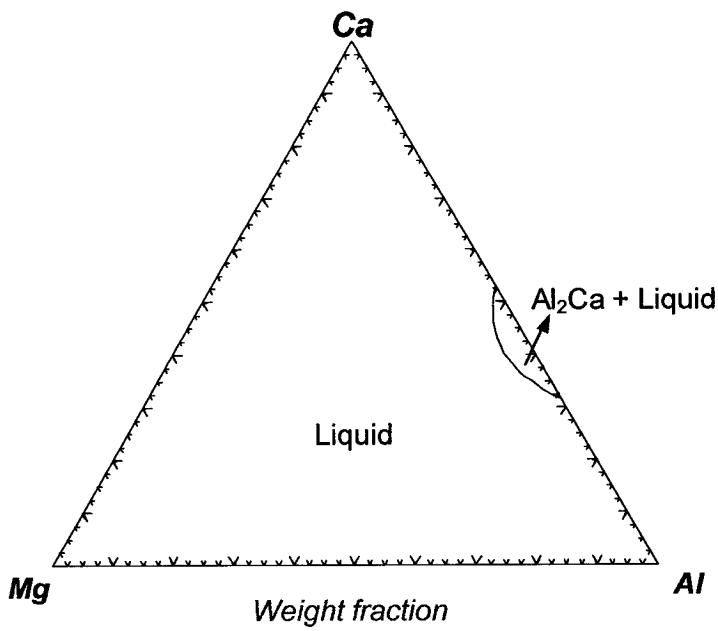

Figure 5.13: *Isothermal section at 1300K*

Prior to solidification at high temperature (above 1360K), the whole concentration triangle is composed of a homogeneous liquid phase and obviously no phase boundaries exist. At 1300K, the primary crystallization of Al_2Ca sets in but is still above the melting

point of the three components. Figure 5.13 shows that besides the region of homogeneous melt, Al_2Ca phase exists in equilibrium with the liquid phase.

Figure 5.14 shows that at 1000K two regions of primary solidification in which crystalline type Al_2Ca and Ca-bcc are in equilibrium with the liquid phase, whereas at 1300K there is only one region (Figure 5.13).

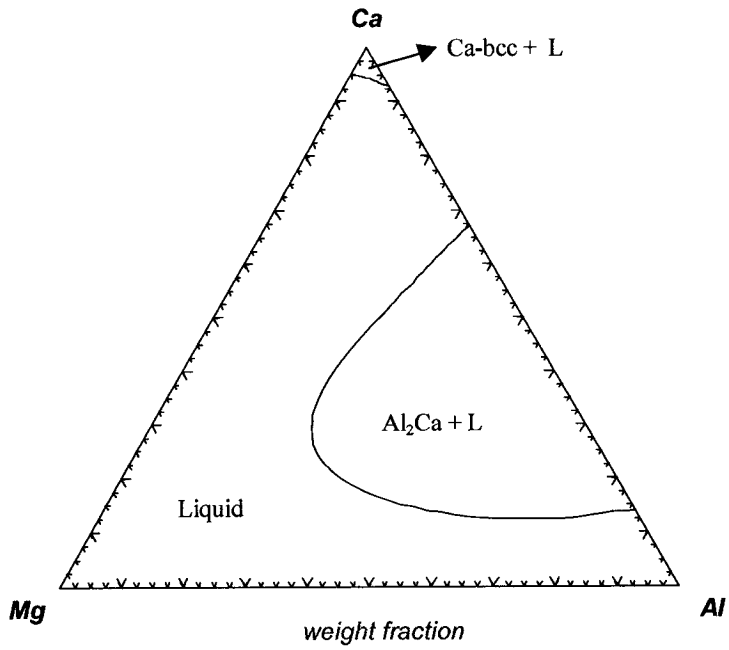

Figure 5.14: *Isothermal section at 1000K*

By cooling from 1000K to 850K further primary solidification of different phases takes place, and instead of two there are ten regions of primary solidification in which the crystalline types, Al_2Ca, Mg_2Ca, $Al_{14}Ca_{13}$, Al_4Ca, (Al), (Mg) and Ca-bcc occur in equilibrium with the liquid phase. The solidification regions are shown in Figure 5.15.

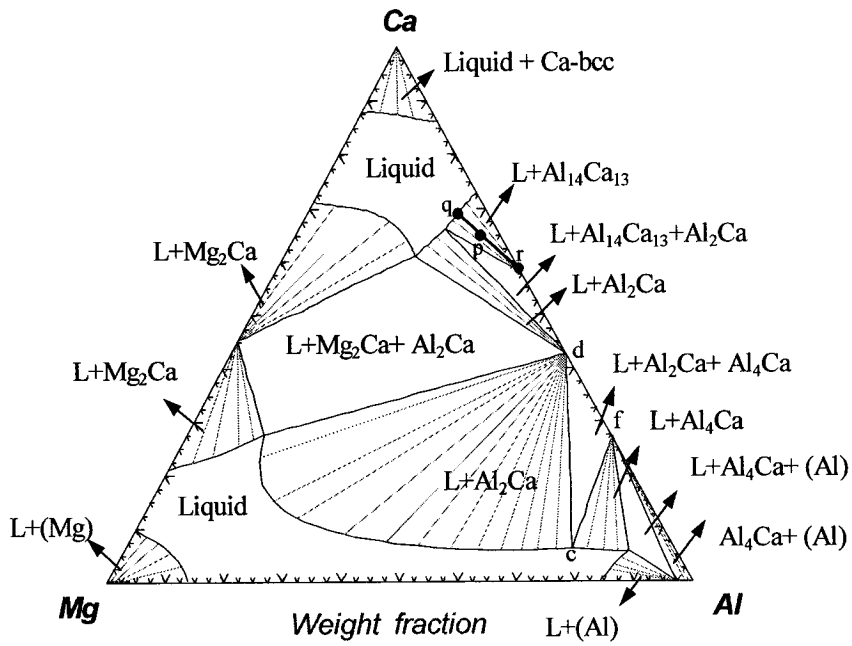

Figure 5.15: *Isothermal section at 850K*

In the isothermal sections, the lines separating regions of primary (i.e L + a crystalline phase) and binary eutectic crystalline (i.e. L + two crystalline phases) must appear as straight lines, since they represent intersections of a horizontal plane (isothermal section) with a surface, which was generated through the motion of a horizontal line, (the eutectic line) [65]. Two binary peritectic and one binary eutectic have been encountered by cooling to 850K, these are:

$$L \rightarrow (Al) + Al_4Ca \quad \text{(eutectic reaction)} \tag{5.1}$$

$$L + Al_2Ca \rightarrow Al_4Ca \quad \text{(peritectic reaction)} \tag{5.2}$$

$$L + Al_2Ca \rightarrow Al_{14}Ca_{13} \quad \text{(peritectic reaction)} \tag{5.3}$$

It is to be noted that if the overall composition lies within two-phase regions, then the compositions of the two phases are given by the ends of the tie line, which passes through the overall composition. For example, a sample with an overall composition *p*, in Figure 5.15 in L+$Al_{14}Ca_{13}$ region, consists of a liquid of composition *q* on the liquidus and a solid $Al_{14}Ca_{13}$ compound of composition r. The relative proportions of the two phases are given by the lever rule:

$$\text{(weight of liquid)/(weight of solid)} = pr \,/\, pq \qquad (5.4)$$

where *pr* and *pq* are the lengths of the tie-line segments. In the case of solid $Al_{14}Ca_{13}$, the solid phase is nearly stoiciometric; so all tie lines of the (L+ $Al_{14}Ca_{13}$) region converge nearly to the corner of the triangle. In the case of (Mg), a very narrow region of solid solubility is observed. At 850K alloys with overall compositions in the two-phase region (Al_4Ca+(Al)) consist of two solid phases. Alloys with overall compositions within the three-phase triangle dcf, consist of three phases: solids Al_2Ca and Al_4Ca with compositions at *d* and *f* respectively and liquid of composition *c*.

Figure 5.16 shows the isothermal section at 750K. It can be seen that the region of the melt shrinks, however at this temperature the liquid is still in equilibrium with the other phases in the two and three phase regions. At this temperature, the binary eutectic point between Ca and Al has been encountered as can be seen from the region of L+Al_3Ca_8+Ca-bcc and is a result of the following eutectic reaction;

$$L \rightarrow Al_3Ca_8 + \text{Ca-bcc} \quad \text{(eutectic reaction)} \qquad (5.5)$$

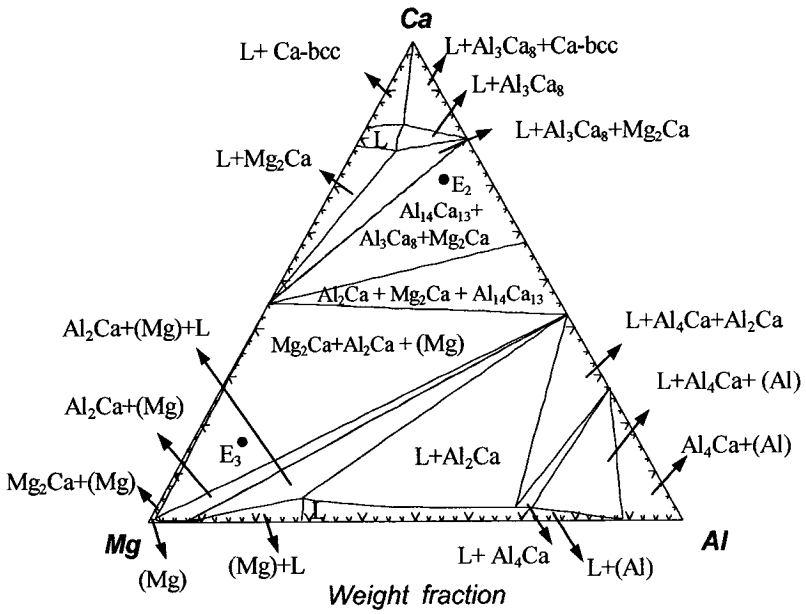

***Figure 5.16**: Isothermal section at 750K*

There are also another eutectic and one peritectic reactions which have been encountered by cooling to 750K. They occur according to the following reactions:

$$L \rightarrow (Al) + Al_4Ca \quad \text{(eutectic reaction)} \qquad (5.6)$$

$$L + Al_2Ca \rightarrow Al_4Ca \quad \text{(peritectic reaction)} \qquad (5.7)$$

There are still regions of primary solidification of Ca-bcc, Al_3Ca_8, Mg_2Ca, Al_2Ca, (Al), (Mg) and Al_4Ca in equilibrium with the melt. Figure 5.16 shows three regions of three-solid phases. Upon cooling near to 750K, two ternary eutectic points (E_2, E_3) have been encountered. The two ternary eutectic reactions are as follows:

E_2: $$L \rightarrow Mg_2Ca + Al_3Ca_8 + Al_{14}Ca_{13} \qquad (5.8)$$

E_3: $$L \rightarrow Mg_2Ca + Al_2Ca + (Mg) \qquad (5.9)$$

A later stage of solidification is shown in Figure 5.17, where there is no residual liquid. At this temperature (700K), there are eight three-crystalline-phases regions and

four two crystalline-phases region. There are four other ternary eutectic points (E_1, E_4, E_5, E_6) that have been encountered upon cooling to 700K, these reactions are:

$$E_1: \quad L \rightarrow Mg_2Ca + Al_3Ca_8 + Ca\text{-fcc} \tag{5.10}$$

$$E_4: \quad L \rightarrow \gamma + Al_2Ca + (Mg) \tag{5.11}$$

$$E_5: \quad L \rightarrow Al_2Ca + \gamma + \beta \tag{5.12}$$

$$E_6: \quad L \rightarrow Al_4Ca + \beta + (Al) \tag{5.13}$$

where the composition of γ and β phases are $Mg_{17}Al_{12}$ and $Al_{140}Mg_{89}$, respectively.

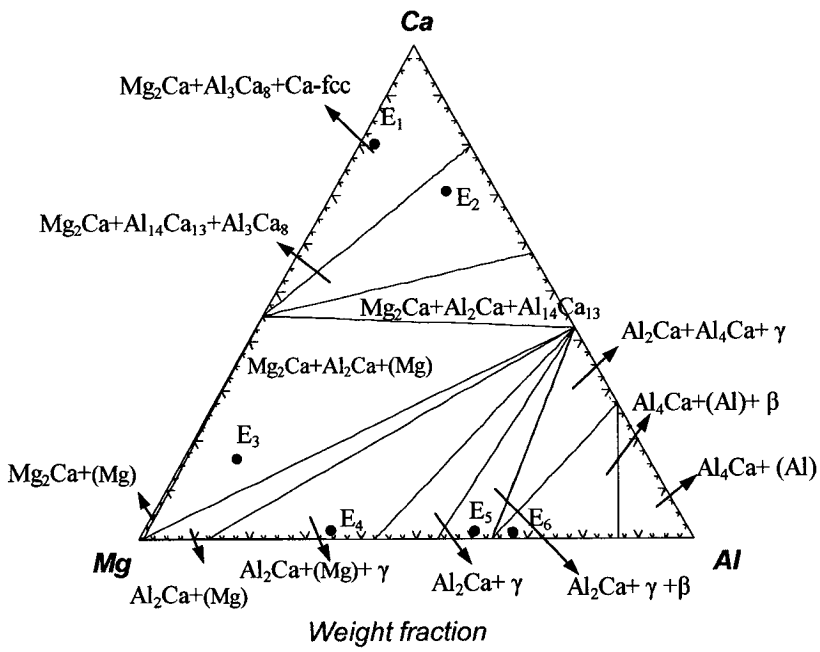

***Figure 5.17**: Isothermal section at 700K*

5.3.2 Liquidus projection of Mg-Al-Ca system

A two dimensional representation of the ternary liquidus surface may be obtained as an orthogonal projection upon the base composition triangle. Such polythermal projection of the liquidus of the Mg-Al-Ca is shown in Figures 5.18 and 5.19 that are based on mole fraction and weight fraction, respectively. These diagrams are calculated by using FactSage 5.2 software with the optimized parameters for the binary systems. The univariant valleys are shown as heavier lines. By convention, the large arrows indicate the directions of decreasing temperature along these lines. As solidification proceeds by precipitation of primary phases, the composition of the liquid changes progressively, and this change is represented by a path on the liquidus projection, occurring in a direction representing a lowering of the temperature on the liquidus surface. Figures 5.18 and 5.19 also show the six ternary eutectic (E_1 to E_6) points, two ternary quasi-peritectic points (P_1 to P_2) and five saddle points (S_1 to S_5). P_1 and P_2 are quasi-peritectic points as on the univariant line two arrows join in and one arrow leaves the invariant point. In the ternary phase diagram, points e_1 to e_8 and p_1 to p_2 indicate the binary eutectic and peritectic points respectively. Calculated ternary invariant points are listed in Tables 5.7 and 5.8 in mole and weight fraction, respectively. There is qualitative agreement between the liquidus projection of Ozturk *et al.* [60] and this calculation. From their experimental result, a detailed XRD and transmission electron microscopy (TEM) investigation suggested that there was an intermetallic phase $(Mg,Al)_2Ca$, which was a ternary solid solution phase. There is disagreement between the calculated ternary phase diagram of this work and Kevorkov *et al.* [8], because they considered a larger ternary solubility for binary phases Mg_2Ca, Al_2Ca and Al_3Ca_8.

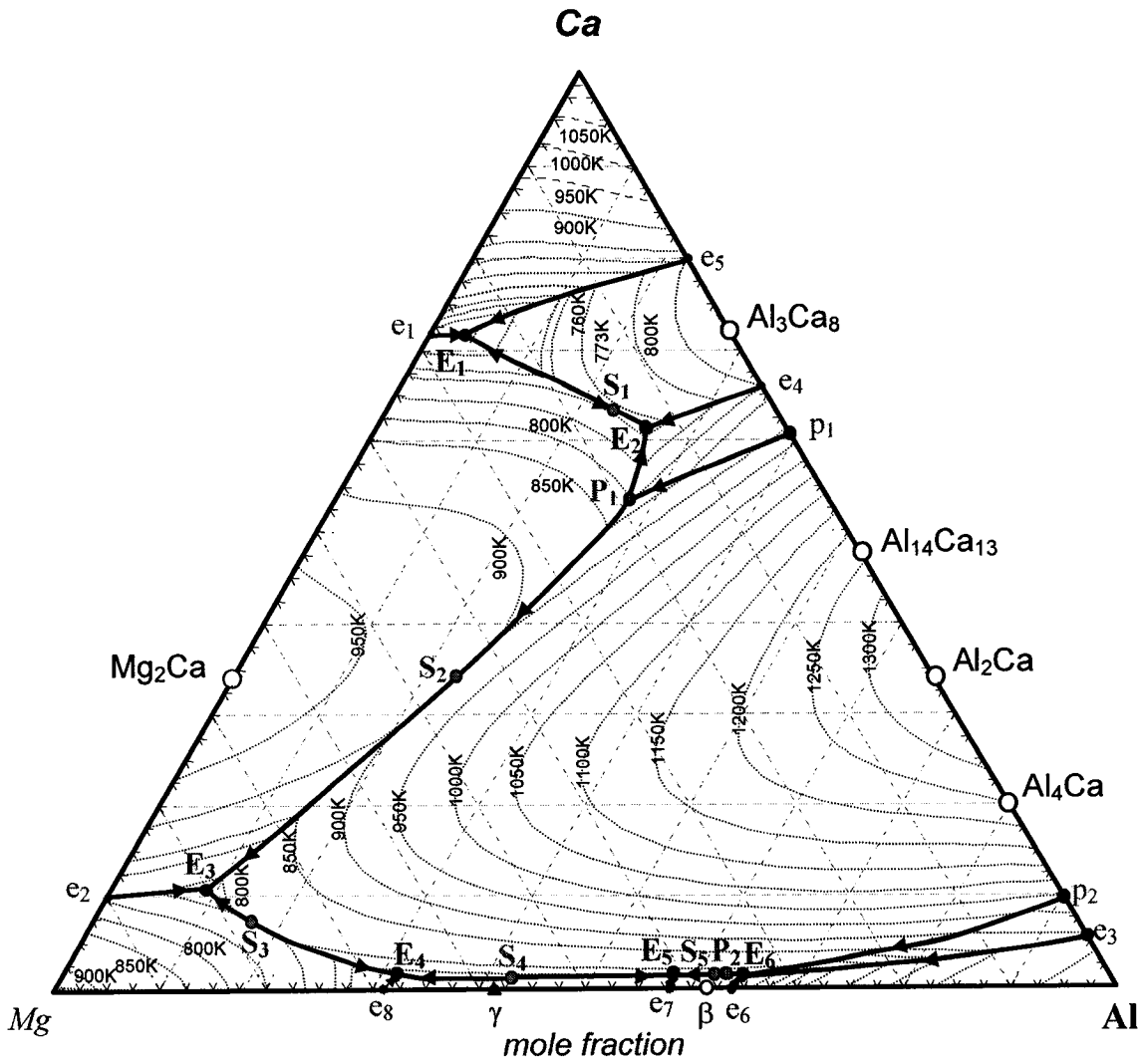

Figure 5.18: *Liquidus projection for Mg-Al-Ca system based on mole fraction*

Comparison with the result of Kevorkov *et al.* [8] is shown in Table 5.7.

Table 5.7: *Calculated invariant points of the Mg-Al-Ca system based on mol%.*

Reaction/ Reaction type	**Temp (K)**	mol% Ca	mol% Mg	mol% Al	Reference
L⟷ Mg_2Ca + Ca-fcc + Al_3Ca_8 / Eutectic E_1	710.54	71.60	25.20	3.20	This work
	717.00	70.00	15.00	15.00	[8]
L ⟷ Mg_2Ca + Al_3Ca_8 + $Al_{14}Ca_{13}$ / Eutectic E_2	764.19	61.20	13.30	25.50	This work
	761.00	58.00	13.00	29.00	[8]
L ⟷ Mg_2Ca + Al_2Ca + (Mg) / Eutectic E_3	754.72	10.90	79.90	9.20	This work
L ⟷ γ + Al_2Ca + (Mg) / Eutectic E_4	701.50	1.20	67.20	31.60	This work
	697.00	2.00	33.00	65.00	[8]
L ⟷ Al_2Ca + γ + β / Eutectic E_5	715.92	1.10	41.20	57.70	This work
L ⟷ Al_4Ca+ (Al)+ β / Eutectic E_6	717.00	1.10	34.70	64.20	This work
	715.00	1.06	34.74	64.20	[8]
L⟷ Mg_2Ca + Al_3Ca_8 / Saddle S_1	768.11	63.20	15.28	21.52	This work
L⟷ Mg_2Ca+Al_2Ca / Saddle S_2	902.96	33.76	45.56	20.68	This work
	1008.00	33.30	30	36.70	[8]
L ⟷ Al_2Ca+ (Mg) / Saddle S_3	773.88	7.48	77.80	14.72	This work
	808.00		78.00 – 79.00		[8]
L ⟷ Al_2Ca + γ / Saddle S_4	723.80	1.26	56.49	42.25	This work
L ⟷ Al_2Ca + β / Saddle S_5	718.37	1.50	37.22	61.28	This work
L + Al_2Ca⟷ $Al_{14}Ca_{13}$+ Mg_2Ca / Ternary Quasi Peritectic P_1	823.89	53.90	18.40	27.70	This work
	777.00	58.00	13.00	29.00	[8]
L+ Al_2Ca⟷ Al_4Ca+ β / Ternary Quasi Peritectic P_2	717.39	1.10	35.60	63.30	This work

For example they reported a calculated eutectic point (E_1) occurring at 444°C according to:

$$L = \text{Ca-bcc} + Mg_2Ca + Al_3Ca_8 \qquad (5.14)$$

Although their model showed the precipitate of Ca-bcc (equation 5.14), their experiments indicate that Ca-fcc forms instead. The current study is in agreement with their experimental results for this eutectic point.

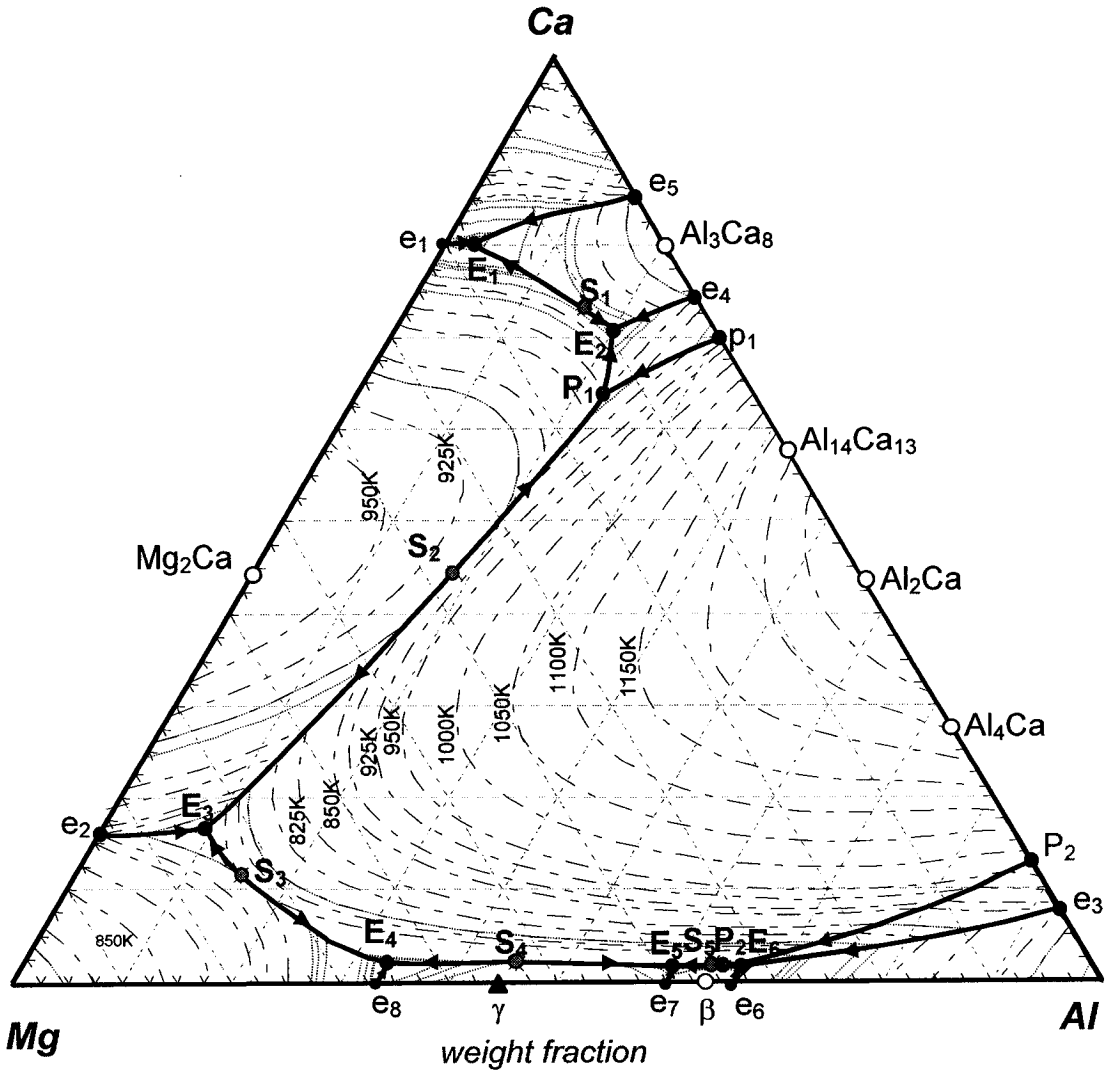

***Figure 5.19**: Liquidus projection for Mg-Al-Ca system based on weight fraction*

The critical points presented in weight percentage are shown in Table 5.8.

***Table 5.8**: Calculated invariant points of the Mg-Al-Ca system based on wt%.*

Reaction / Reaction type	Temp (K)	wt% Ca	wt% Mg	wt% Al
L ⟷ Mg_2Ca + Ca-fcc + Al_3Ca_8 / Eutectic E_1	710.00	80.44	17.28	2.28
L ⟷ Mg_2Ca + Al_3Ca_8 + $Al_{14}Ca_{13}$ / Eutectic E_2	764.31	70.87	9.29	19.84
L ⟷ Mg_2Ca + Al_2Ca + (Mg) / Eutectic E_3	755.00	16.66	74.03	9.31
L ⟷ γ + Al_2Ca + (Mg) / Eutectic E_4	701.76	1.88	64.62	33.50
L ⟷ Al_2Ca + γ + β / Eutectic E_5	715.40	1.57	38.53	59.90
L ⟷ Al_4Ca+ (Al) +β / Eutectic E_6	716.98	1.57	32.30	66.13
L ⟷ Mg_2Ca+Al_3Ca_8 / Saddle S_1	768.11	73.09	10.82	16.09
L ⟷ Mg_2Ca+Al_2Ca / Saddle S_2	902.96	44.31	35.95	19.74
L ⟷ Al_2Ca+ (Mg) / Saddle S_3	773.88	11.50	73.34	15.15
L ⟷ Al_2Ca + γ / Saddle S_4	723.80	2.05	52.85	45.10
L ⟷ Al_2Ca + β / Saddle S_5	718.37	1.85	34.92	63.23
L+Al_2Ca ⟷ $Al_{14}Ca_{13}$+Mg_2Ca / Ternary Quasi Peritectic P_1	823.89	63.78	13.57	22.65
L+Al_2Ca ⟷ Al_4Ca + β / Ternary Quasi Peritectic P_2	717.39	1.76	33.99	64.25

5.3.3 Isopleth diagram

One of the benefits of establishing thermodynamic database for a multi-component system is the ability to calculate or obtain different diagrams, which provide details about the alloy or composition under question. It also provides the phase relations at different temperature and the effect of the content of constituent components on phase equilibria. For example a vertical section for a particular composition such as 70.87 wt.% Ca through the space model shows phase transformation for that composition (Figure 5.20). It is important to note that on an isopleth the tie lines do not, in general, lie in the plane of the diagram. Therefore, the diagram provides information only on which phases are present, not on their compositions. The boundary lines on an isopleth do not in

general indicate the phase compositions, only the temperature at which a phase appears or disappears for a given overall composition. The lever rule cannot be applied on an isopleth. For example, if we consider the cooling from the liquid state of an alloy at composition *a*, we will find that, at T = 854.6K, precipitation of the solid $Al_{14}Ca_{13}$ phase begins. At T = 802.4 K (point *b* in Figure 5.20) the solid Al_3Ca_8 phase begins to appear. Finally at eutectic temperature T_E, the ternary reaction occurs, leaving solid Al_3Ca_8, $Al_{14}Ca_{13}$, Mg_2Ca at lower temperatures.

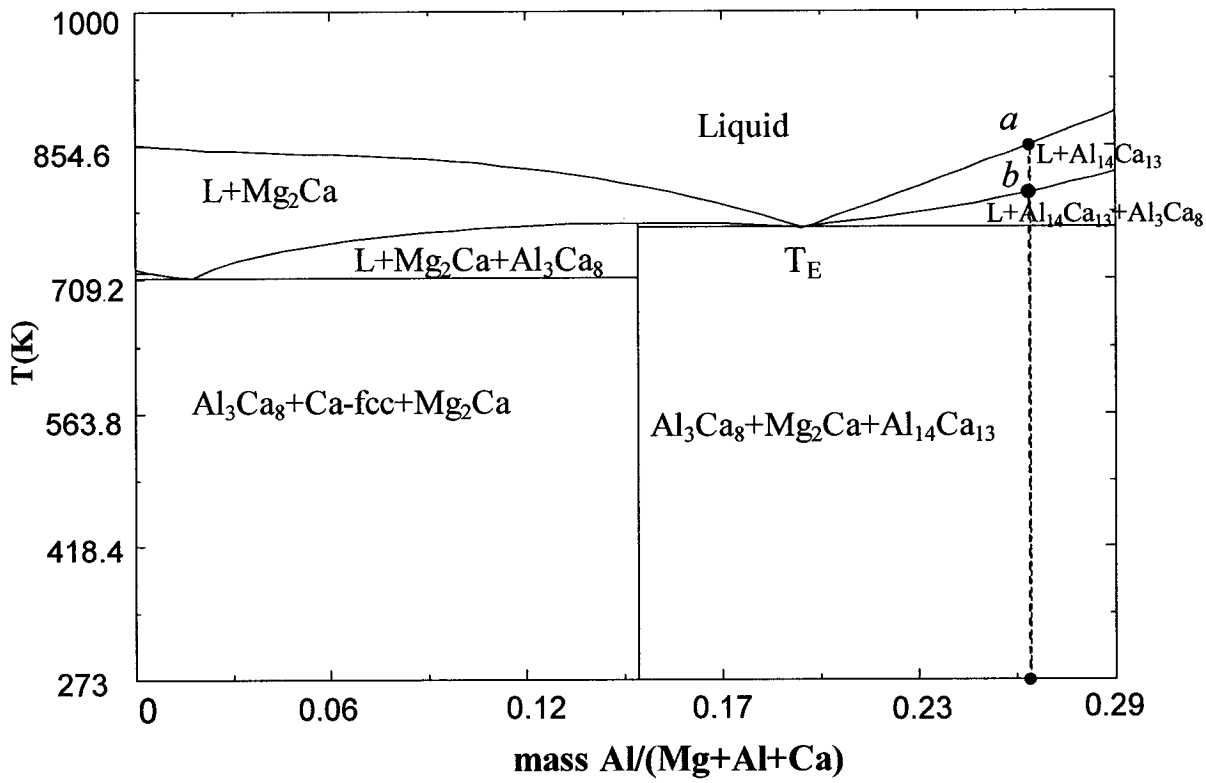

Figure 5.20: *Isopleth (constant composition section) of the Mg-Ca-Al system at P=1 bar at 70.87 wt% Ca*

5.3.4 Phase assemblage diagram

As mentioned above, the isothermal sections of ternary diagrams show the phases in equilibrium and their composition at various temperatures. However, they do not show the relative amount of each phase and formation and/or decomposition temperature of these phases. For this purpose phase assemblage diagram can be drawn where phase distribution, versus temperature can be calculated from the database. In order to explain the benefit of these diagrams an example is discussed in this section.

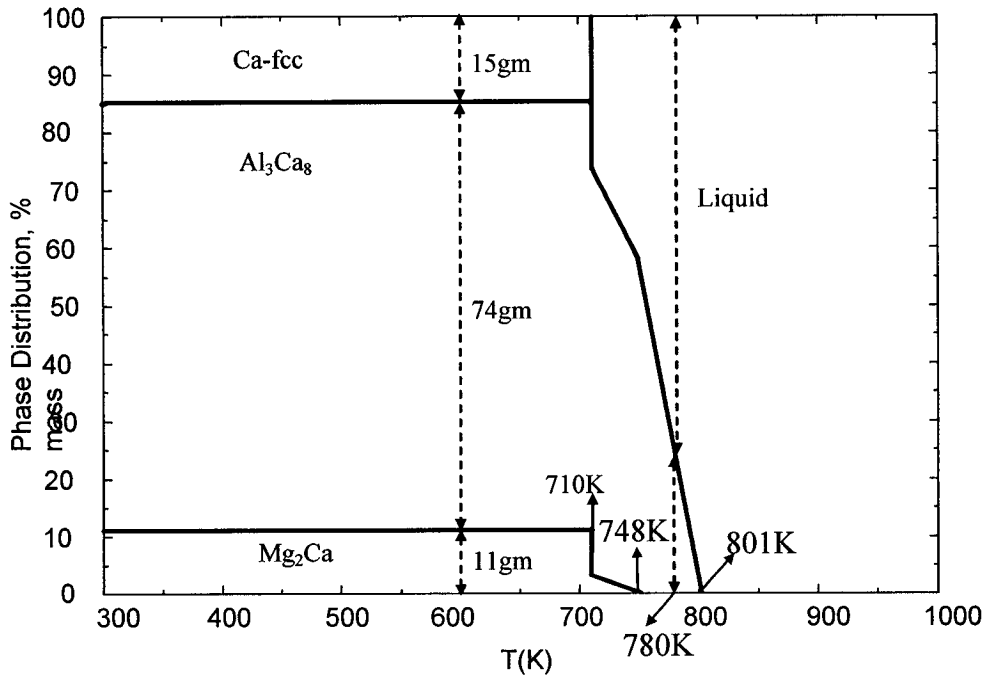

Figure 5.21: *Phase assemblage of (71 mol% Ca, 9 mol % Mg, 20 mol% Al) composition*

Figure 5.21 is calculated for an alloy composed of 71 mol% Ca, 9 mol % Mg, 20 mol% Al. The proportion of different phases at any working temperature can easily be read from this figure. For instance, at 780 K, 100 gm of the overall material consists of 23 gm of Al_3Ca_8 and 77 gm of liquid. It can be seen from this figure that Al_3Ca_8 is the first

solid to precipitate in this alloy upon cooling. It starts precipitation at 801K, whereas Mg_2Ca and Ca-fcc start to precipitate at 748K and 710K, respectively. This figure also gives the phase proportion of this alloy at room temperature after solidification. Below 710K the proportion of solids remains constant with decreasing temperature. For example at 600K there are 11 gm of Mg_2Ca, 74 gm of Al_3Ca_8, 15 gm of Ca-fcc which remain constant down to room temperature.

CHAPTER VI

Conclusions

6.1 Summery

In this research Mg-Al-Ca system was thermodynamically modeled and from the results the following conclusions are drawn.

- Phase equilibria and thermodynamic data for binary systems were evaluated and optimized with available data to obtain one set of self-consistent model parameters for the Gibbs energy of all phases as function of temperature and composition.
- The Redlich-Ksiter polynomial model was used for the calculation of excess Gibbs energy for liquid and solid solution phases.
- Minimum number of optimized thermodynamic coefficients was used to calculate the phase diagram and other integral and partial thermodynamic properties such as activities, enthalpy of mixing, partial Gibbs free energy and partial enthalpy, which reproduced the experimental measured values very well.
- The optimized model parameters can also be used to predict thermodynamic properties, which are not available in the literature.
- By combining self-consistent set of model equations for the Gibbs energy of the phases of the three binary systems, the ternary Mg-Ca-Al phase diagram was

obtained. Here it is assumed that there is no ternary solubility between the binary compounds due to the lack of experimental data. No ternary interaction parameters or terms were introduced either since no ternary thermodynamic data are available.

- In the Mg-Ca-Al ternary system six ternary eutectic points in the temperature range of 701 K to 764 K and two peritectic points in the temperature range 717 K to 825 K and five saddle points in the temperature range of 724 K to 904 K were found.
- There is a difference between experimental results of Kevorkov *et al.* [8] and the results of this study because they considered ternary solid solubility and AlCa stoichometric compound instead of $Al_{14}Ca_{13}$.

6.2 Contributions

Ozturk *et al.* [60] and Kevorkov *et al.* [8] conducted extensive experimental work and thermodynamic calculations on the Mg-Al-Ca system. But there is no instance of a detailed (compositions and temperatures of eutectic points) and complete ternary phase diagram for Mg-Al-Ca system. Moreover they used Agarwal *et al.* [18] results for optimization of the Mg-Ca system that used a higher number of parameters. In the current study, the number of parameters has been reduced for the Mg-Ca system, and the Al-Ca system is reoptimized taking $Al_{14}Ca_{13}$ as the compound instead of AlCa. Moreover for the two binary systems developed in this study, the phase diagram and the thermodynamic properties are in good agreement with experimental results found in the literature. By combining the three binary systems a complete ternary phase diagram with

all possible invariant points has been obtained. More importantly the model parameters obtained in this study are made available for the development of Mg multi component thermodynamic database.

6.3 Suggestions for future work

For the Mg-Al-Ca ternary system this work is a step to more complete evaluation and refinement that could be extended by the availability of new experimental results and by the addition of other components like Sr, Si etc.

The existence of ternary compounds and ternary solid solubility is yet to be verified experimentally.

References

[1] Humble P., "Toward a cheap creep resistant magnesium alloy", *Material forum,* **21**, pp. 45-56, 1997.

[2] Greenfield P., "Magnesium", Mills and Boo Limited, London, pp. 7-19, 1972.

[3] Kainer U. K. (editor), "Magnesium-alloys and technologies", Willy-VCH, in German, pp. 1-7, 72-73, pp. 108-110, 2003.

[4] Luo A. A., Balogh M. P., Powell B. R., "Creep and microstructure of magnesium-aluminum-calcium based alloys", *Metallurgical and Materials Transactions A*, **33**(A), pp. 557-574, 2002.

[5] Ozturk K., Zhong Y., Liu Z-K., "Computational thermodynamics and experimental investigation of Mg-Al-Ca alloys", *TMS*, pp. 113-117, 2001.

[6] Alico J., "Introduction to magnesium and its alloys", Ziff-Davis publishing company, Chicago.New York, pp. 38-42, 1966.

[7] Ozturk K., Zhong Y., Liu Z-K., "Computational thermodynamics and experimental investigation of the Mg-Al-Ca-Sr alloys", *TMS (The materials, Metals & Material society)*, pp. 69-73, 2002.

[8] Gröbner J., Kevorkov D., Chumak I., Schmic-Fetzer R., "Experimental investigation and thermodynamic calculation of ternary Al-Ca-Mg phase equilibria", *Ternary phase equilibria*, pp. 1-22, 2003.

[9] Pekguleryuz M. O, Renaud J., "Creep resistance in Mg-Al-Ca casting alloys", *Magnesium 2000 Symposium, TMS*, pp. 279-84, 2000.

[10] Pekguleryuz M., "Development of creep resistant Mg-Al-Sr alloys", *The Minerals, Metals and Material society*, pp. 11-15, 2003.

[11] Liu Z-K., "Understanding magnesium alloys through computational thermodynamic", *TMS*, pp. 205-213, 2002.

[12] Baar N., "On the alloys of molybdenum with nickel, manganese with thallium, and calcium with magneisum, Thallium, Lead, Copper, and Silver", *Z. Anorg. Allg. Chem.*, **70**, pp.362-366, 1911. [From British Library www.bl.uk, "Ca-Mg (Calcium-Magnesium)", Landolt-Bornstein Series IV/5c, pp. 22-25]

[13] Paris R., "Contribution on the ternary alloys", Publ. Sci et Tech Ministére Air (France), **45**, pp. 39-41, 1934. (Cited in [17])

[14] Haughton J. L., "Alloys of magnesium. Part 6 – The construction of the magnesium-rich alloys of magnesium and calcium", *J. Inst Met.*, **61**, pp. 241-246, 1937. (Cited in [18])

[15] Vosskühler H., "The phase diagram of magnesium-rich Mg-Ca alloys", *Z. MetallKd,* **29**, pp. 236-237, 1937. (Cited in [17])

[16] Klemm W., Dinkelacker F., "On the behavior of magnesium with calcium, strontium, and barium", *Z. Anorg. Chem.*, **255**, pp. 2-12, 1947. (Cited in [17])

[17] Nayeb-Hashemi A. A., Clark J. B., "The Ca-Mg (calcium-magnesium) system", *Bull. Alloy phase diagrams*, **8,** pp. 58-65, 1987.

[18] Agarwal R., Lee J., Lukas H. and Sommer F., "Calometric measurements and thermodynamic optimization of the Ca-Mg system", *Z. Metallkd.*, **86**(2), pp. 103-108, 1995.

[19] Chase M. W., "Heat of transition of the elements", *Bull. of Alloy phase diagrams*, **4**(1), pp. 123-124, 1983.

[20] Burke E. C, "Solid solubility of calcium in magnesium", Trnas. *AIME* , **203**, pp. 285-286, 1955. (Cited in [18])

[21] King R. C., Kleepaa O. J., "A thermodynamic study of some selected laves phases", *Acta Metall.*, **12**, pp. 87-97, 1964.

[22] Davison J. E., Smith J. F., "Enthalpy of formation of $CaMg_2$", *Trans. Met. Soc AIME*, **242**, pp. 2045-2049, 1968.

[23] Hultgren R., Desai P. D., Hawkins D. T., Gleiser M., Kelley K. K., "Selected values of the thermodynamic properties of binary alloys", *ASM*, Metals Park, OH, 1973. (Cited in [25])

[24] Sommer F., Predel B., and Assmann D., "Thermodynamic investigation of liquid alloys in the systems Mg-Ca, Mg-Sr, and Mg-Ba", *Z. Metallkd.*, **68**(5), pp. 347-349, 1977.

[25] Mishra P. P., Milanarun M., Jha N., Mishra A. K., "Thermodynamic properties of liquid glass-forming Ca-Mg alloys", *Journal of Alloys and Compounds*, **340,** pp. 108-113, 2002.

[26] Sommer F., "Thermodynamic activities of liquid alloys in the system Ca-Mg using a modified ruff method", *Z. MetallKd.*, **70**(8), pp. 545-547, 1979.

[27] Mashovets V. P., Puchkov L. V., "Vapor pressure over molten alloys in the system Mg-Ca", *Zh. Prikl. Khim.,* **38**(5), pp. 1009-1014, 1965. [Cited in (17)]

[28] Matsuyama K., "On the equilibrium diagram of the Al-Ca system", Sci. Reports Tohoku University **17**, pp. 783-789, 1928. (Cited in [29])

[29] Kevorkov D., Schmid-Fetzer R., "The Al-Ca system, Part 1: experimental investigation of phase equilibria and crystal structures", *Z. Metallkde*, **92**, pp. 946-952, 2001.

[30] Kevorkov D., Schmid-Fetzer R., Pisch A., Hodaj F., Colinet C., "The Al-Ca system, Part 2: calorimetric measurements and thermodynamic assessment", *Z. Metallkde*, **92**, pp. 953-958, 2001.

[31] Huang B. Q., Corbett J. D., "Two new binary calcium-aluminum compounds: $Ca_{13}Al_{14}$, with a novel two-dimensional aluminum network, and Ca_8Al_3, and Fe_2Al type analogue", *Inorganic Chemistry*, **27**(22), pp. 5827-5833, 1998.

[32] Ozturk K., Chen L-Q, Liu Z-K, "Thermodynamic assessment of the Al-Ca binary system using random solution and associate models", *J. alloys and compounds*, **340**, pp. 199-206, 2002.

[33] Nowotny H., Wormnes E., Mohrnheim E., "Investigation on the Al-Ca, Mg-Ca and Mg-Zr systems", *Z. Metallkd*, **32**, pp. 39-42, 1940.

[34] Itkin V. P., Alcock C. B., Ekeren Van P. J., Oonk H. A. J, "The Al-Ca (aluminum-calcium) system", *Bull. Alloy Phase Diagrams,* **9**, pp. 652-657, 1988.

[35] Notin M., Gachon J. C., Hertz J., "Enthalpy of formation of Al_4Ca and Al_2Ca and of the liquid alloys (aluminum+calcium)", *J. Chem. Thermodynamcis*, **14**(5), pp. 425-434, 1982.

[36] Sommer F., Lee J. J., Predel B., "Thermodynamic investigations of liquid Al-Ca, Al-Sr, Mg-Ni and Ca-Ni alloys", *Z. Metallkd,* **74**(2), pp. 100-104, 1983.

[37] Jacob K. T., Srikanth S., Waseda Y., "Activities, concentration fluctuations and complexing in liquid Ca-Al alloys", *Trans. Jpn. Inst. Met.,* **29**, pp. 50-59, 1988. (Cited in [29])

[38] Schürmann E., Fünders C .P., Litterscheidt H., "Vapor presseure of Ca above Ca-Si, Ca-Al and Ca-Al-Si alloys", *Arch. Eisenhuttenews.*, **46**, pp. 473-476, 1975. (Cited in [32])

[39] Notin M., Gachon J. C., Hertz J., "Thermodynamic data for calcium-based alloys from a new galvanic method," *CALPHAD*, **6**(1), pp. 49-56, 1982.

[40] Murray J. L, "The Al-Mg (aluminum-magnesium) system", *Bull. Alloy Phase Diagrams*", **3**(1), pp. 60-74, 1982.

[41] Löüdecke D., Hack K., "A thermodynamic evaluation of the Al-Mg system", *Z. Metallkd.,* **77**, pp. 145-161,1986.

[42] Saunders N., "A review and thermodynamic assessment of the Al-Mg and Mg-Li systems", *CALPHAD*, **14**(1), pp. 61-70, 1990.

[43] Zuo Y., Chang Y. A., "Thermodynamic calculation of the Al-Mg phase diagram", *Calphad,* **17**(2), pp. 161-174, 1993.

[44] Chartrand P., Pelton A. D., "Critical evaluation and optimization of the thermodynamic properties and phase diagrams of the Al-Mg, Al-Sr, Mg-Sr, and Al-Mg-Sr systems", *Journal of phase equilibria,* **15**(6), pp. 591-605, 1994.

[45] Goel N. C., Cahoon J. R., Mikkelsen, "An experimental technique for the rapid determination of binary phase diagram: the Al-Mg system", *Metallurgical Transactions A.*, **20**(A), pp. 197-203, 1998.

[46] Moser Z., Katayama I., Fukuda Y., "New thermodynamic data for liquid aluminum-magnesium alloys from emf, vapor pressure and calorimetric studies", *Journal of phase equilibria*, **19**(1), pp. 38-47, 1998.

[47] Su H. L., Harmelin M., Donnadieu P., Baetzner C., Seifert H. J., Lukas H. L., Effenberg G., and Aldinger F., "Experimental investigation of the Mg-Al phase diagram from 47 to 63 at.%", *Journal of Alloy Compound.*, **247**, pp. 57-65, 1997.

[48] Liang P., Su H. L., Donnadieu P., Harmelin M., Quivy A., "Experimental investigation and thermodynamic calculaiton of the central part of the Mg-Al phase diagram", *Z. Metallkde*, **89**(8), pp. 536-40, 1998.

[49] Donnadieu, P., Harmelin M., Seifert H. J., Aldinger F., "Commensurately modulated stable states related to the gamma phase in Mg-Al alloys", *Philos. Mag. A,* **78**(4), pp. 893-905, 1998.

[50] Czeppe T., Zakulski W., Bielanska E., "Study of the thermal stability of phases in the Mg-Al system", *Journal of phase equilibria*, **24**(3), pp. 294-254, 2003.

[51] Ozturk K., Luo A. , "Phase identification and microanalysis in the Mg-Al-Ca alloy system", *The Minerals and Materials Society (TMS),* pp. 195-200, 2003.

[52] Wenwen D., Yangshan S., "Microstructure and mechanical properties of Mg-Al based alloy with calcium and rare earth additions", *Materials Science and Engineering,* **356**, pp. 1-7, 2003.

[53] Ansara I., Dinsdale A. T., Rand M. H.,"COST 507 – Thermochemical database for light metal alloys", European Commission EUR 18499, 1998.

[54] Portnoi K. I., Spektorova S. I., Express information B, **19**(5), 1948. (Cited in [55])

[55] Prince A., "Aluminum – Calcium – Magnesium", in Ternary alloys: a comprehensive compendium of evaluated constitutional date and phase diagram, **3**, pp. 611-614, 1988.

[56] Dow Chemical Co. Midland, MI, "Liquidus determinations of polynary magnesium alloys", Dow Chemical Co. Report 15004, U.S. Govt. Res. Reports 31, pp. 355,1959. (Cited in [8])

[57] Catterall J. A., Pleasance R. J., "The constitution of Mg-rich Mg-Al-Ca alloys", *J. Inst Met.*, **86**, pp. 189-192, 1957. (Cited in [55])

[58] Stacey R. D., "Some primary phases in the Mg-Al-Ca system", U.K. Atomic Energy Authority, Industrial Group Report, R&DB(S) TN-2167, 1958. (Cited in [8])

[59] Tkachenko V. G., Khoruzhaya V. G., Meleshevich K. A., Karpets M. V., and Frizel V. V., "Physicochemical and structural investigation of materials", *Powder metallurgy and Metal Ceramics*, **42**(5-6), 2003.

[60] Ozturk K, Zhong Y, Luo A., Liu Z-K, "Creep resistant Mg-Al-Ca alloys: computational thermodynamics and experimental investigation", *Jom*, **55**(11), pp. 40-44, 2003.

[61] Ursula R. K., "Thermodynamic modeling of multi-component phase equilibria", *National Institute of Standards and Technology, JOM,* **49**(12), pp. 14-19, 1997.

[62] Yan X-Y, Zhang F., Chang Y. A., "A thermodynamic analysis of the Mg-Si system", *Journal of phase equilibria,* **21**(4), pp.379-384, 1999.

[63] Cahn R. W. (Editors), Haasen P., Kramer E. J., "Material science and technology-a comprehensive treatment", VCH: Weinheim., New York, Basel, Cambridge, **5**, pp. 1-75, 1991.

[64] Hertz J., "Josiah Willard Gibbs and teaching thermodynamics of materials (History)", *Journal of phase equilibria*, **5**(13), pp. 450-458, 1992.

[65] Mamoun M., "Phase Equilibria in theAlN-Al_2O_3-Y_2O_3 systems-Utility in AlN processing", PhD thesis, McGill University, Montreal, QC, 2001.

[66] Kaufman L., Bernstein H., "Computer calculation of phase diagrams with special reference to refractory metals," Academic Press, New York, NY, 1970. (Cited in [61])

[67] Loehman R. E., "Characterization of ceramics", Butter Worth-Heinemann, 1993. (Cited in [65])

[68] Lukas H. L., Henig Th., Zimmermann B., "Optimization of phase diagrams by a least-squares method using simultaneously different types of data", *CALPHAD*, **3**(1), pp. 225-236, 1977.

[69] "Thermodynamic of phase diagrams", http://www.sv.vt.edu

[70] Dinsdale A. T., "Thermodynamic data of the elements", *CALPHAD*, **15**, pp. 317-425, 1991.

[71] Bale C. W., Pelton A.D., "Optimization of binary thermodynamic and phase diagram data", *Metall. Mater. Trans. B*, 14(B), pp. 77-83, 1983.

[72] Pelton A. D., Bale W. C., "Legendre polynomial expansions of thermodynamic properties of binary solutions", *Metallurgical Transactions A*, **17**(A), pp. 1057-1063, 1986.

[73] "WinPhad 2.0 – Phase diagram calculation engine for binary systems," CompuTherm LLC, Madison, WI, USA, 2000.

[74] "FactSage 5.2", Thermfact (Centre for research in computational thermochemistry), Montreal, QC, Canada, 2003.

[75] Bergeron and Risbud, "Introduction to phase equilibria in ceramics", *The American ceramic society*, Inc. Reading, 1994.

[76] Gordon P., "Principles of phase diagrams in materials systems", McGraw-Hill, Inc., New York, 1968. (Cited in [77])

[77] Rao Y. K, "Principles of phase diagrams. phase diagrams, material science and technology", Vol:1, Theory, principles and techniques of phase diagrams. A.M. Alper (ed), Academic press, USA, pp. 1-43, 1970.

[78] Cottrell A. H., "An introduction to metallurgy", St. Martin's press, New York, 1967. (Cited in [77])